The Pennsylvania State University

The Graduate School

FIELD DEPLOYABLE GUIDED WAVE TRASNDUCERS FOR HIGH-TEMPERATURE APPLICATIONS

A Thesis in

Engineering Science and Mechanics

by

Yamankumar P. Trivedi

Submitted in Partial Fulfillment
of the Requirements
for the Degree of

Master of Science

August 2019

The thesis of Yamankumar P Trivedi was reviewed and approved* by the following:

Cliff J. Lissenden
Professor of Engineering Science and Mechanics Advisor
Thesis Advisor

Andrea Arguelles
Professor of Engineering Science and Mechanics

Parisa Shokouhi
Professor of Engineering Science and Mechanics

Judith A. Todd
P. B. Breneman Department Chair
Head of the Department of Engineering Science and Mechanics

*Signatures are on file in the Graduate School.

Abstract

Degradation is a natural phenomenon that can occur in all materials, if undetected it can lead to structural failure. Thus, there is a crucial need to monitor structures exposed to some external stimuli. This lays the foundation for Nondestructive Evaluation and Structural Health Monitoring. Both approaches provide the means and information needed to detect the advance of damage. Of the multitude of techniques used in NDE or SHM, ultrasonic testing is perhaps the most common. The wide range of excitation methods and the ability to control the waves through various means account for its popularity. Transducers, which convert the energy from one form to another, facilitate the generation and detection of ultrasonic waves. However, the field-testing of structures at high-temperature is a challenge, as commercial transducers are often not suitable for such high-temperatures.

Deposition and processing techniques for temperature-tolerant piezoelectric film transducers that are appropriate for field installation on metal structures with minimal need for heating the substrate are developed and tested. The direct bond of the film to the structure precludes the use of couplants. Film coatings have served various NDE purposes, where previous work investigated the use of sol-gel, potato starch and single crystal films. Herein, the ferroelectrics Bismuth Titanate and Lithium Niobate are investigated. The film consists of a piezoelectric powder, a lithium-silicate based high-temperature inorganic binding agent and water. Electrodes are installed on the top of the film and then it is poled. To show the viability of these films, pulse-echo, temperature testing and capacitance measurements are performed to characterize the films. Bismuth titanate films are also processed as comb transducers to send and receive guided waves, and for the first time Lamb waves are generated and received from this type of air-sprayed transducer.

Table of Contents

List of figures

List of Tables

Acknowledgements

This work would not have been possible without the support of two of my advisers. Dr Bernhard Tittmann first provided the insight and motivation for this project as it was in his Lab all the previous work in the use of Bismuth Titanate for the film transducer technology. Dr Cliff Lissenden has been very supportive and has always pushed me to bring the best out of me. He has been very patient with me, even when I was difficult to work with. In the research labs and groups of both the professors, I was able to research at my own pace and freedom. Without their expert advice and guidance, this work would not been possible. The experience I had during this thesis has been eye-opening, full with curiosity and enjoyable as a whole.

I appreciate everything my friends and family have done to support me through this. I would like to specifically thank Sonark, Ashwin, Shreya, Sanat, Sarthak, Matt, Bryan and Nishit. They have helped me through my good and bad times and lighten up difficult times to give the power to get past them.A special thanks to all the researchers preceding and laying the groundwork for this work. Work by Ledford and Xu laid the foundation for the use of Bismuth Titanate while Cho and Lesky's work provided insight for the use of comb transducers. I would like to thank my current and previous lab mates Caio, Joe, Ray, Janet, Velika, Chaitanya and Anurup. A special thanks goes to Chris Hakoda for helping me immensely towards to final stages to help me in finishing the work. Finally, I would like to thank my committee for providing their input and making this a better project overall.

Dedication

This Thesis is dedicated to my Parents without whom I would not be who and where I am.

Chapter 1 – Introduction

1.1 Problem Statement

The United States has the largest network of pipelines in the world, with more than 2.5 million miles of pipes. Their major uses are for the transportation and distribution of energy products, such as crude oil, petroleum, and natural gas. Also, many of the infamous leak-based tragedies such as the Deepwater Horizon spill, Bhopal gas tragedy, and the nuclear leak at Sellafield, UK are related to piping systems. All of these, and many other tragedies, have been due to lax safety precautions and inadequate monitoring tools. These accidents led to a loss of valuable resources, loss or injury of lives and severe environmental impacts. Incidents such as these illustrate the importance of nondestructive evaluation (NDE) and structural health monitoring (SHM) to detect material degradation in structures. Furthermore, these incidents happened under extreme conditions, which is another important element of performing SHM. Currently, inspections are performed offline (e.g., by shutting down the power plant periodically) due to the lack of workable testing equipment under higher temperatures. In the case of nuclear power plants, there is an urgent need for optimization of their operational reliability. Extended operation periods and newer reactor designs have called for better safety strategies and lesser maintenance efforts. This has led to a rising need for online health monitoring of these structures. A pragmatic system would be setup to observe the system, periodically note response measurements, approximate the remaining useful life and inform about abnormalities when needed. Metals are the most used materials in the energy industry for obvious reasons. Their material properties, chemical reactivity and temperature resistance could be molded as desired in order to perform the necessary tasks, some of the structures in the energy industry are shown in Figure 1.1.

Figure 1.1: Structures in the energy industry where SHM is needed for active systems such as pipelines as well as storage tanks [43] [44] [46]

Most of the common sensors for ultrasonic NDE and SHM are made up of PZT (lead zirconate titanate) which has a very limited range of operating temperatures (<150 ^{o}C). The need for better high-temperature sensing systems has led many researchers to investigate better designs and materials. There are multiple environmental factors taken into consideration apart from temperature. Humidity, target specimen, sunlight, electrical charges, natural frequency (resonance) are just a few of the other factors to keep in mind when preparing a high-temperature sensing system. One of the biggest drivers for better piezoelectric materials is the low Curie temperature of PZT. Curie temperature is the temperature at which a material loses its electric and magnetic properties, after which the material will not show any ferroelectricity, piezoelectricity or pyroelectricity [4]. Curie temperatures of some common piezo materials are listed in Table 1.1.

Table 1.1: Curie Temperature and Piezoelectric Coefficient of common piezo materials

Material	*Curie Temperature (^{o}C)*	*Piezo Coefficient d_{33} (pC/N)*
PZT	200 [35]	590 [35]
Bismuth Titanate	670 [36]	40 [36]
Lithium Niobate	1150 [41]	31 [37]
PVDF	195 [40]	20 [38]
Barium Titanate	120 [35]	190 [35]

This thesis research continues the effort to develop transducers for ultrasonic NDE/SHM in elevated temperature environments. The transducers are permanently affixed to the structure to enable on-line condition monitoring using a spray deposition technique. The use of Bismuth Titanate (a high-temperature piezoceramic) is not new, however, the spray deposition process is quite novel. It eliminates the need for high temperature couplant and enables use on surfaces that are not flat. Another high-temperature piezoelectric coating investigated in this thesis is a mixture of Lithium Niobate and Barium Titanate. These transducer materials are investigated due to their elevated temperature capabilities. However, the research objective of this thesis is to show that piezoelectric coating spray-on transducers are capable of sending and receiving ultrasonic guided waves. To this end, Lamb waves in plates and shells are generated and received. The remainder of this chapter provides background information on piezoelectricity, ultrasonic transducers, wave propagation in solid media, and nondestructive evaluation / structural health monitoring. Then Chapter 2 provides a review of spray-on transducer deposition and some fundamentals of guided wave propagation.

Chapter 3 describes the processing of thick film transducers for this research. It provides the material properties of the piezoceramics employed in the transducer fabrication. Bismuth Titanate and Lithium Niobate are investigated as elevated temperature tolerant alternatives to PZT. The transducers are deposited on to a sample and poled to impart piezoelectricity. Post poling, pulse-echo measurements are obtained and the transducers are subjected to an elevated temperature in a furnace. Signal to Noise ratio, and the piezoelectric coefficient (d_{33}) is recorded along with the capacitance and dielectric constant. Another novel technique suggested in this thesis is the use of organic solvents instead of inorganic solvents. Some film characterization of this design is also presented.

The key results are given in Chapter 4, which describes the experimental procedures and results obtained for guided wave generation and reception in plates. Conclusions and future work suggestions are provided in Chapter 5.

1.2 Piezoelectricity

The word Piezoelectric is derived from the Greek *piezein*, which translates to squeeze or press and piezo means to push. The piezoelectric effect is the ability of certain materials to generate an electric charge in response to an applied mechanical stress. Piezoelectric materials exhibit a direct piezoelectric effect (generation of electricity due to applied stress) and a converse/reversible effect (mechanical strain due to an electric charge). When stress is applied to a crystal, it undergoes strain and a difference of potential is generated between opposing faces. Piezoelectric materials can detect sound at frequencies up to 10^{12} Hz and can be used for excitation through the inverse effect. Piezoelectric materials couple the electrical and mechanical effects, which is described through mathematical equations. Constitutive equations can better quantify the behavior of piezoelectric materials. Here S is the mechanical strain, T is mechanical stress, E is the electric field and D is the electric displacement

$$S = s^E T + d E$$

$$D = d T + \varepsilon^T E.$$

In a non-piezoelectric material, electric displacement, D, comes solely from an applied electric field, E, and not from an applied stress, T. Similarly, in a non-piezoelectric material, strain, S, comes solely from an applied stress, T, and not from an applied electric field, E. However, in a piezoelectric material, an applied electric field and an applied stress both impart some electric displacement. The other coefficients, d, ε^T, s^E quantify the degree of contribution of the applied potentials to the displacements. The coefficient, d, is the piezoelectric constant as it is a measure of the strength of the piezoelectric effect of the material. When considering the use of the material in which the applied voltage and measured strain are along the same axis (z-axis, or 3-axis), the piezoelectric constant for this case is the d_{33} and is a common quantity used to describe the performance of the material. There are multiple ways for exciting ultrasonic waves such as piezoelectricity, electrostriction, magnetostriction, EMAT, laser, etc. The majority of the work done so far investigates the use of a piezoelectric material as it can serve as a transmitter and a receiver.

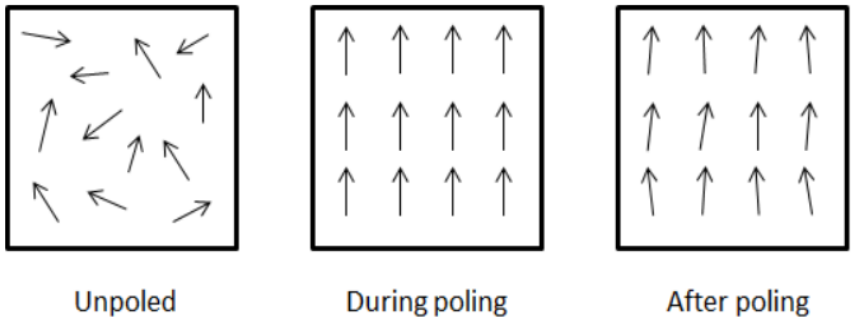

Figure 1.2: Orientation of the electric dipoles in a material [42]

There are materials which naturally exhibit piezoelectricity such as Quartz, Rochelle salt and Lead Titanate, but materials such as PZT, Barium Titanate and Lithium Niobate are synthesized to provide higher performance. Ferroelectric materials are often times considered as a subset within the piezoelectric world. Ferroelectrics are those materials whose electric dipole moments could be oriented with an electric field in a desired configuration [21]. Most ferroelectric materials could be oriented to perform as a piezoelectric; however, the efficiency greatly depends on its lattice structure. The dipoles are randomly arranged as shown in Figure 1.2 and must be coerced into a polarized alignment [8]. The time and the strength of the electric field depends on the material and is generally quantified as the coercive field. For the poling of bulk materials, an electric field is imparted around them at a field intensity of the coercive field or higher. Most materials possess the ability to be polarized, but only ferroelectrics retain the polarization once the field is removed. The remnant polarization in these materials is what facilitates the piezoelectric effect to occur. Factors such as the element thickness, remnant polarization and the conditions they are applied to determine the life of these sensors as there is a degradation over time due to their induced polarity. Some alternatives for improved sensitivity have been researched, but they have low operating temperatures and are very expensive to produce.

1.3 Ultrasonic Transducers

Ultrasonic transducers convert electrical energy into mechanical vibrations (sound waves) for actuation and sounds waves into electrical energy for sensing. A subset is said to be electro-acoustic transducers, as the presence of a piezoelectric material is what allows the

energy conversion. The piezoelectric material converts energy between the electrical, mechanical and acoustical domains. The piezoelectric element is generally supported by other elements of a transducer such as the backing layer, casing, coax-cables etc. and it together forms a piezoelectric transducer as shown in Figure 1.3. Every element has a mechanical resonance frequency based on its thickness, density and stiffness. Generally, the transducer excitation is designed to match the frequency of their element when operating. The mechanism by which this change of energy domain occurs could be achieved through various means. Movable magnets in an electrical coil or the use of variable capacitance is very common in the loudspeaker and audible sound industry, however, the generation of ultrasonic waves through the use of piezoelectric transducers is mainly discussed here [8].

Any element (single-crystal, composite, ceramic or polymer) that can exhibit the piezoelectric effect, is potentially used for transducer application. Single-crystal is made up entirely of a continuous crystal lattice. As they have a perfect orientation and maximum polarization, they do not need to be poled. Polycrystalline piezoceramics are agglomerates of single-crystals, where each crystal has a unique orientation. Even though this generally has a lower performance, materials which cannot be grown as a single-crystal be used if they are polarized. A Piezopolymer utilizes organic materials that possess piezoelectric properties [5].

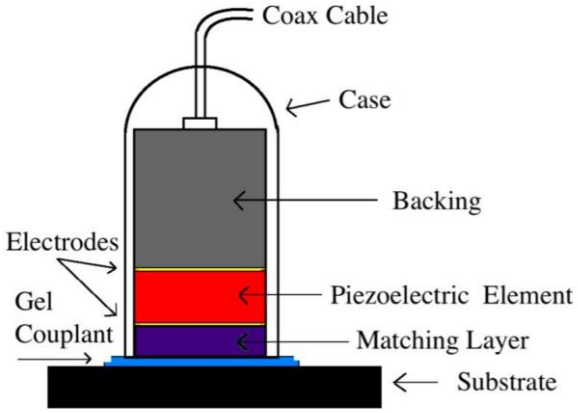

Figure 1.3: Single Crystal acoustic transducer [8]

For a typical single-crystal element shown in Figure 1.3, there are a few other layers between the active element and the target specimen, such as the impedance matching layer and

backing layer. The matching layer is generally designed to be between the piezoelectric element and the target specimen for the waves to undergo a less sudden mismatch of acoustic impedance. This allows a more efficient acoustic energy transfer into the target specimen. The backing layer which is a highly attenuating layer is present on the rear side of the element to reduce the element ringing and to shorten the element's impulse response. Shortening the impulse response increases the element's sensitivity to a wider band of responses [22]. A couplant (typically water or gel based) is then used to further decrease the impedance mismatch from the sensor to the substrate and further assists the matching layer in obtaining the highest possible transfer of the acoustic energy.

1.4 Wave Propagation in Solid Media

Sound at high frequency (ultrasonic) has been used in the field of Nondestructive testing (NDT) and Structural health monitoring (SHM) for more than 60 years now. Ultrasonic Testing consists of techniques that use short bursts of high-frequency ultrasonic waves to identify abnormalities in a material. Although the techniques and theory can be complicated, the concept is very simple. Unlike electromagnetic waves, sound waves need a medium to propagate in. The goal is to understand the wave interaction with the solid and represent it quantitatively. Ultrasonic waves (frequency around 20kHz or higher) are passed into an object and when these waves interact with the object boundaries, they either deviate from their propagation direction or are reflected back. For controlled transmission of ultrasonic waves, transducer devices are used. Transducers are instruments that convert energy from one form to the other, and most ultrasonic transducers rely on the piezoelectric effect for wave generation. In NDE applications, frequencies typically range from 50 kHz to several GHz. For industrial applications, ultrasonic testing is widely used for metals, plastics, composites and ceramics, however, it is not suitable for wood and paper products.

Considering sound in general for humans, it can be associated as anything we hear through air; however, sound waves propagate through solids and liquids as well, which is contrary to what we know about the electromagnetic (light) waves. In reality, sound waves in solid media actually travel faster and with a lower loss of energy compared to air. Through these

waves, we can use their features such as velocity and attenuation to characterize a material and its properties. For NDE purposes, we use the echo properties of a transmitted wave which reflect from a flaw, to determine the size, shape, and position of a flaw. There are many sub-categories within the field of ultrasonic testing such as reflective (pulse-echo) testing, guided wave testing (angle or phased array), laser detection and acoustic emissions testing. Depending on the application, appropriate evaluation techniques are chosen. For example, for bridge inspection, acoustic emission testing is a preferred method while for large pipes and plates, guided wave testing might be optimum. In the power industry, most structures are made from metals due to their long life and high melting points. The components are primarily found in a pipe or plate geometry. The wave propagation in particular structures used in this thesis will be discussed in Chapter 2.

Figure 1.4: Longitudinal and Transversal wave vibration [6]

Elasticity is a solid's ability to deform and then restore its shape and volume after the end of an applied external force. Considering the wave motion in a taut string with a finite length, using Newton's second law for an elementary volume, we can derive the longitudinal wave equation in an elastic solid. The one-dimensional, homogenous wave equation is:

$$\frac{\partial^2 u}{\partial x^2} c^2 = \frac{\partial^2 u}{\partial t^2}$$

Where $c = \sqrt{F/\rho}$ and u is the particle displacement in the x direction. This wave equation assumes plane wave propagation only and ignores any dispersion effects. From the wave equation, it has been shown that waves can propagate as two types of modes having different velocities in infinite solid media. In longitudinal wave propagation, the particle vibration is in the direction of propagation with an expanding-contracting wave motion. In transverse waves, the vibration is perpendicular to the propagation caused by shear deformations as shown in Figure 1.4. Both methods of propagation are important to study as elastic waves

have been a corner stone for the investigation of the initiation and propagation of damage and fractures.

1.5 Nondestructive Evaluation and Structural Health Monitoring

There is an expanding role for nondestructive evaluation techniques in almost every field such as manufacturing, energy, infrastructure, industries, and even the field of research and development. The study of material fracture has existed for centuries as even during Roman times, the way a particular glass piece broke gave them information about different fracture modes in glass. This helped them fabricate sturdier and reliable glassware, which is utilized for daily purposes. Plenty of information related to fracture mechanics is readily available, as compared to NDE or SHM which are relatively new fields. SHM is based on a similar idea of NDE, where materials are tested for anomalies, which hamper their performance. However, SHM methods relies on the continuous monitoring of a structure for an extended period. With the help of periodic-active or continuous passive monitoring, technicians can generate an understanding of the deteriorating state of a material and the conditions that may cause the degradation. The cost to manufacture, install and operate a new component is time-consuming and expensive, hence the concept for periodic assessment aids in preparing a better component.

Figure 1.5: NDE of a pipe section using a hand held ultrasonic transducer [45]

NDE approaches have a clear use depending on the material and geometry of the specimen. Conventional NDE finds its use at in-situ inspection for structures such as railway lines, pipelines, protective coatings, and other crack detection. For many complex structures such as aircraft, bridges, NDE has evolved towards the use of smart structures. The advent of the composite materials has facilitated this evolution by enabling sensors to be embedded during manufacturing. Modern signal processing techniques have also improved from the original pulse-echo techniques. Now it's possible to recover buried signals, and approaches such as neural network signal processing are improving the NDE world. Previous students and researchers associated with our research group have used varied methods for the inspection of materials. Among the many NDE/SHM systems, suitable methods are chosen depending on the component, it's accessibility, surrounding conditions, etc. The use of film spray-on sensors is an SHM approach used for this research, as the sensors are developed for continuous monitoring and data collection for an extended period of time.

Chapter 2 – Literature Review

This chapter provides some insight in the film sensor technology and fabrication procedures that has given rise to the techniques used in Chapter 3 and 4. The earlier part of this chapter reviews previous work conducted by researchers in this field and the work of various students at the Pennsylvania State University. The later part of the chapter provides some guided wave propagation theory important for topics covered in chapter 4.

2.1 Film Transducers

The work in the field of preparing film transducers has only recently gained some momentum. Limitations in fabrication methods have prevented the creation of efficient film transducers. Of the various thick-film transducers discussed, there are drawbacks associated with each method. Research on piezomaterials has gained interest in a plethora of applications in fields such as electronics, biology, electrical engineering, architecture and medicine. One of the most used materials is PZT, which is known for its high dielectric constant, good electrochemical coupling and piezoelectric coefficient. However, due its brittle nature, the ceramic is difficult to properly bond to a surface. A solution to this problem is to create a mixture where PZT is doped with another material. Work has been done with materials such as Bismuth Titanate (used primarily in this research), Lithium Niobate etc. PVDF is a widely used piezopolymer that is chemically inert and creep resistant. It also has a wide frequency range, but has a low piezoelectric coefficient. Due to this reason, a composite mixture of PZT and PVDF could provide the advantages of both in the transducer [23].

Alternatives such as Aluminum Nitride (AlN) have proved to be useful for testing at high-temperatures due to its high curie temperature [39]. Aluminum Nitride has a broad frequency operating bandwidth when used as a film transducer [52]. A lot of work done on AlN is for its capability for electronic applications such as resonators, optoelectronic elements and surface acoustic wave devices but not much on exploiting its use for high-temperature NDT applications. The reason for that is oxidization of the AlN films at higher temperatures and

their expensive fabrication. PVDF films by themselves are great due to their flexibility and ready availability. If prepared as an interdigitated transducer (IDT) along with laser electrode patterning, the electrodes could be shaped anyway and the films can serve many purposes [24]. As they could be prepared as films and connected to a material, they are already polarized, which drastically simplifies the fabrication procedure.

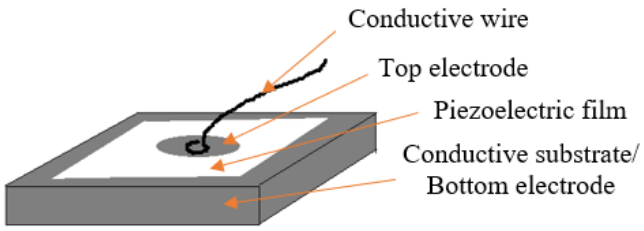

Figure 2.1: Thick Film Spray-on Transducers

Film transducers, such as shown in the schematic of Figure 2.1, have served as a basis for characterization and testing of materials, however due to their complex fabrication procedure, they can be difficult to deploy for field testing. Through recent work done by previous researchers and in this thesis, it is shown that there is a reasonably straight forward method to field apply film transducers. Other factors such as durability and environmental tolerance will have to be studied in the future to properly benchmark the longevity of the films, but temperature characterization is performed in this thesis. Research done at Penn State has assessed Bismuth Titanate as the piezopowder and the primary objective was to create a transducer system comparable to a monolithic commercial transducer in functional ability. This was achieved by numerous experimental trials for the materials and fabrication methods. The novelties associated with this research are that the processing route is field-deployable and the transducer is capable of generating and receiving ultrasonic guided waves.

2.2 Previous Work in Film Ultrasonic Transducers

The use of thin-film ultrasonic transducers was first presented by Barrow through the creation of PZT sol-gel transducers, followed by high-temperature sol-gel transducers by

Kobayashi. Research in film transducer processing was continued by many researchers and students at Penn State. Key aspects of their work relevant to the current study are discussed here.

A sol-gel mixture consists of solid particles in micrometer sizes dispersed into a liquid where the suspension is naturally facilitated by the Brownian motion. The particles are so small that sedimentation doesn't occur. This solution is then applied onto a surface by a suitable deposition technique. The particles in the sol are polymerized through the removal of stabilizing components and a gel remains attached to the surface of deposition [53]. Sol-gel mixtures have been found to be used for thin coatings of a given metal oxide. This technology has proved useful against corrosion and can create high-purity as well as quality coatings. To form thick coatings, either layers could be added or larger particle powders loaded into the sol-gel. Special caution will have to be taken to ensure there is no sedimentation, but this possibility was exploited by research to create ferroelectric ceramics. The mixture is prepared by heating the slurry to particular temperatures in order to remove any organic components. Previously, Sol-gel fabrication yielded an average thickness of 10 microns, however, Barrow [14] decided to use heavier ceramic powders such as lead zirconate titante (PZT) and was successfully able to fabricate films at least 200 microns in thickness.

Barrow laid the foundation in the development and characterization of a thick film, lead zirconate Titnate (PZT) sol-gel composite by following the sol-gel method established by Yi [25]. In this method, a dispersed solution is applied to the sample, sintered and annealed, allowing it to strongly bond to the sample surface. This created crack-free films of relatively larger thickness than previously. Barrow's work paved a way for other piezoceramics to be investigated and soon the material that is studied in this research (Bismuth Titanate) was used as a piezoelectric film by Kobayashi [15]. Their method suggested the use of bulk ceramic powders with higher operating temperatures. The sol-gel mixture was air-brushed on samples and high-temperature tests with platinum electrodes were recorded to prove the validity of their use. Kobayashi's research quickly became adopted for the non-destructive evaluation and guided wave applications at Penn State. Searfass was the first one to evaluate the potential of Bismuth Titanate/PZT sol-gel transducers for high-temperature applications

[12]. Sinding then studied the effect of weight percentage of BiT/PZT powder on the transducer properties [26]; Orr studied the bond stiffness and Malarich suggested a method to fabricate comb-transducers in the field with limited success [11] [27].

As the sol-gel mixture contains acetic acid, the films are reactive substances and subsequently perform poorly on carbon steel and iron substrates due to corrosion. Thus, an alternative method was suggested by Ledford [8], where he developed two new transducers, one using starch as a binder and the other using an inorganic industrial binder. Both had working functionality, however the inorganic binder makes the film compatible for usage at higher temperatures. Furthermore, the deposition was by brush rather than spray-on.

Ledford's transducers were created with Bismuth Titanate powder, Ceramabind 830 and water. However, the binder concentration was too high, which required thicker films and longer fabrication time. He performed some initial tests where the films were deposited on a sample and the substrate was heated to 330 ^{o}C where it was held at that temperature for 100 hours. The signal strength appeared to improve due to the heat-treatment initially, and then was stable for the remaining time. This was due to the densification of the film and removal of moisture and impurities. Xu then studied the use of Lithium Niobate/Barium Titanate as films to create transducers for even higher temperatures. Lithium Niobate and Aluminum Nitride tend to oxidize and render the film useless at higher temperatures [9]. Although, by mixing Barium Titanate with Lithium Niobate, it was found that even though there was a loss of signal strength at higher temperatures due to the oxidation, the transducer was still operating.

Xu [9] was able to identify the optimum fabrication procedure and conditions that resulted in the Bismuth Titanate transducer film that is studied in this thesis. A parallel team of researchers working in a similar direction, but without the thick films, form the basis for the later part of this thesis. Guided wave research has been performed at Penn State under Rose and Lissenden in the last two decades and there has been work on surface-bonded transducers. Borigo [16] showed the excitation spectrum and mode excitability analysis of comb transducers, followed by Lesky [10] who studied the use of PZT strip transducers to monitor a curved shell structure, and then Cho [7] worked with PVDF to show its utility as a comb transducer when exciting a particular mode. The work of Malarich [11] and Ledford

[8] have provided the direct foundation for this research as they developed a fieldable technique to deposit piezoelectric coatings tolerant of elevated temperatures on non-flat metal surfaces without significant application of heat. Additionally, Lesky's and Cho's research provides a baseline for comparison and a structure on which to deposit the transducers.

2.3 Deposition Techniques

Film transducers for piezoelectric applications work the best if the specimen is conductive so that the specimen can be the ground electrode; fortunately, most materials used in the power industry are metals or their alloys. However, the slurry can adhere differently to various surfaces due to the surface tension of the particles. Therefore, it is important to employ the best deposition method for the task and the material at hand. The methods are relatively straightforward and some yield better results, but not one technique is superior to the other. Methods such as spin-coating, slurry coating, spray-painting, chemical vapor deposition, hydrothermal method, tape-casting, dip coating and ink-jet processing are all widely used for film preparation. Summaries of the methods important to the current work are provided below.

2.3.1 Tape and Dip Casting

Many applications of piezoelectric material require thin sheets for sensors, buzzers, dot-matrix, membrane filters and other microelectronic devices. This requires an optimization of the cold consolidation process and Tape-casting method is able to fabricate thin sheets. As these are thin sheets, a number of dispersants may be used. For PZT and Alumina thin films, the powder is suspended into a MEK-EtOH (Methyl-Ethyl Ketone and absolute Ethanol) solvent along with a dispersant. Work has been performed on utilizing glycerol trioleate, oligomeric polyester, phosphate ester and polyvinylpyrrolidone as deflocculants. The powder is first ball-milled in the solvent and the deflocculant, after which a binder is added. The binders commonly used are polyvinylbutyral (PVB) and butlybenzyl phthalate (BBP). The mixture is again ball-milled (generally using a zirconia milling media) for about

20 hours [54]. The slurry is then tape-cast onto a moving Mylar support and blades are used to shape them after which they are allowed to dry at room temperature in a controlled humidity setting to avoid cracking [17]. The tape can be easily stripped after they have dried and inserted into a furnace for sintering. Here the films are heated up to at least 600 ^{o}C and 1100 ^{o}C in some cases after which they are allowed to cool down. Thickness tests are performed along the way and final tape casts of less than 100 microns were obtained. These membranes are of uniform thickness and provide some flexibility to control the membrane characteristics depending on the initial particle size and the fabrication (mainly powder dispersion and sintering). This controls the green density which in-turn affects its characteristics [17]. The films could then be used as free-standing wafers or bonded onto a surface with some binder. This method of tape-casting as noted above was detrimental in preparing the organic film transducers discussed in section 3.3.

Sol-gel thick films could also be manufactured with dip-coating where the deposition surface is dipped into the slurry. A conventional method, it is many times used to create intermediate layers. Unlike tape-casting, the slurry could be water-based or ethanol based to produce high viscosity films. In some cases, dip coating is employed for a top protective layer to prevent cracking during drying. Further heat treatment may be needed to calcinate the top layer and densify the film [18]. The obtained thickness from dip-coating is dependent on the dipping time and the viscosity of the slurry (or slip as it is sometimes referred as). This slip generally is less viscous than other techniques where the dip time and the repetitions are crucial. Resulting in a very low thickness, the dip method has to be often repeated which add a lot of unknown variables. Sometimes, the process is repeated about 100 times in order to get the desired thickness. The multiple dip-coating process can be used to create thick films where the properties are only a bit different than bulk PZT, potentially due to the difference in thermal processing [19]. Both of these methods are suitable for sol-gel techniques as they use some thermal treatment, however, for film preparation without the sintering step require some other methods.

2.3.2 Paint and Spray-on

Painting is one of the earliest approaches for not only creating film-coating but also piezoceramics. These piezoceramics are colloidal in nature as the mixture is typically made of the piezo-powder and a solvent mixture. For many materials, heat is a big challenge for film formation. If there is a sintering step involved, the materials have to able to withstand high temperatures, which makes the techniques discussed in the earlier section harder to use. For high-temperature purposes, a specific binder is selected to affirm the adhesion of the film on the substrate. The paint technique is very easy as it can be used for all applications and even for tight spots. The slurry could either be painted on with a brush or just splashed on and then distributed as uniformly as possible with some instrument (brush, flat slate, sponge etc.). Depending on the mixture and the deposition material, post-application steps are followed. Similar to the paint method, the slurry could also be sprayed on. A major drawback with the paint method is its inability to control the film thickness and its uniformity. Based on the surface tension of the slurry, the film could be uneven causing the film to have unreliable properties. In the spray-on method, the slurry could be uniformly deposited in a surface area and thickness could more or less be controlled based on the spray pressure and the number of spray repetitions. The process is straightforward and only slightly more tedious than the paint method, however, the post deposition processes can be complicated. In the field of medicine and biology, piezoelectric ink-jet printing is a powerful prototyping technique. MEMS (micro-electro-mechanical systems) constructed piezo ink-jet print heads employ a patterned PZT transducer which is bonded to a silicon diaphragm to generate acoustic energy [20].

2.4 Ultrasonic Guided Wave Propagation

Many structural components, such as plates, shells, and pipes are natural waveguides in which ultrasound can propagate relatively long distances. In addition, many of these structures have large domains that are inaccessible, except to guided waves. Therefore, the use of ultrasonic guided waves is an important part of SHM. Guided waves are becoming

more common due to their faster inspection of large structures. There are some very obvious advantages of the guided wave testing methods over the standard normal beam inspection such as its ability to inspect over long distances. Through the mode and frequency tuning, excellent overall detection could be performed for a short period of time or as an active monitoring system [28].

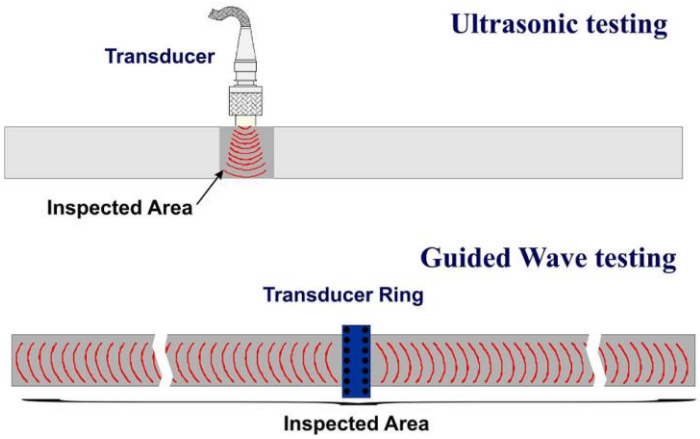

Figure 2.2: Bulk wave ultrasonic detection vs Guided wave detection [47]

2.4.1 History and Background

The field of guided waves has been booming for about past three decades and can be seen more frequently in research and industry. Guided waves provide great opportunities due to the existence of several guided wave modes and frequencies. Researchers have made advancements in utilizing mode and frequency selection to solve many engineering problems. The name guided waves is quite self-explanatory, as the waves are propagated inside a material where they use the boundary of the material to propagate as shown in Figure 2.2.

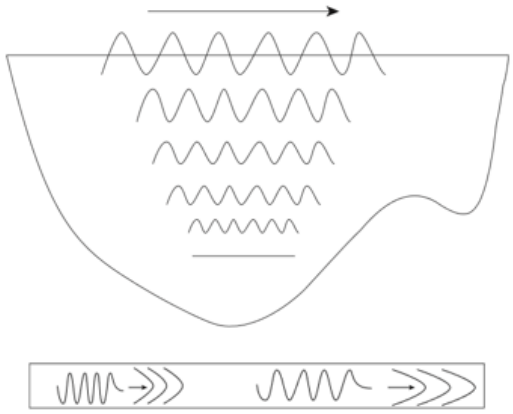

Figure 2.3: Rayleigh surface waves in an infinite half-space at a decreasing amplitude with depth and Lamb waves propagating in a plate [1]

The history of guided waves dates back to Lord Rayleigh and his work performed in the 1880s, which has served as a basis for this industry for about a century. He showed that the surface acoustic waves were the dominant acoustic signal triggered by earthquakes. Rayleigh waves are not only a part of seismology, but also other areas. With the rise of interdigital transducers (IDT), the use of Rayleigh waves has become a part of modern electronics in the form of filters, delay lines, acoustic and electronic applications. Rayleigh waves are one of the simplest cases of guided waves [13]. Rayleigh waves are waves that propagate along the free surface of a semi-infinite isotropic solid (see Figure 2.3). Here the traction forces vanish on the surface and the intensity decreases with depth. They are confined to a range of roughly one wavelength from the propagation surface. Another type of guided wave is the Lamb wave. Lamb waves are plane strain waves that occur in a free plate, where the traction forces vanish on the upper and lower surface of the plate [2] as shown in Figure 2.3.

Bulk waves and guided waves are governed by the same wave equations, the only difference being that the bulk waves do not have to fulfill any boundary conditions while the guided waves do. Now for a pipe geometry, there are innumerable guided wave modes which can be classified as torsional, longitudinal, and flexural modes. The acoustic properties of a wave mode are dependent on the pipe geometry, material and frequency used. With the use of tools and mathematical modeling, dispersion curves are prepared that aid in understanding the wave propagation characteristics better. For commercial guided-wave testing of

pipelines, an array of low-frequency transducers is attached around the circumference of a pipe to generate axially symmetric waves that propagates in both forward and backward directions of the transducer. The transducer functions as a transmitter and a receiver and provides information to the operator. The information can then be represented in many different ways (A-scan, C-scan, FFT etc.).

2.4.2 Mathematical Relations

As described by Achenbach 1984, a free plate problem with prescribed boundary conditions is to determine the propagating modes and their characteristics. The solution is split into Symmetric and Antisymmetric modes that propagate in the plate. To obtain the solution to the symmetrical and antisymmetrical modes, one must consider a traction-free plate as shown in Figure 2.4.

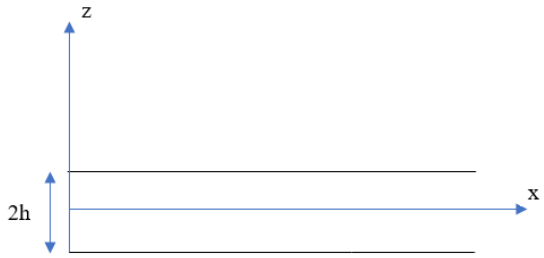

Figure 2.4: Geometry of a free plate problem

The solution for each mode has been shown by Rose [1] through the method of potentials as well as partial waves. The thickness of the plate and the frequency of the mode govern the speed of propagation. For the mode displacement in the x-z plane, the Raleigh-Lamb dispersion equation are:

$$\frac{\tan(qh)}{\tan(ph)} = \frac{-4k^2pq}{(q^2-k^2)^2} \qquad \text{for symmetric modes}$$

$$\frac{\tan(qh)}{\tan(ph)} = \frac{-(q^2-k^2)^2}{4k^2pq} \qquad \text{for antisymmetric modes}$$

Where,

$$p^2 = \left(\frac{\omega}{C_L}\right)^2 - k^2 \qquad \text{and} \qquad q^2 = \left(\frac{\omega}{C_T}\right)^2 - k^2$$

Here, k is the wavenumber equal to ω/C_p and C_p is the phase velocity. The phase velocity is the speed of a wave that will propagate in a particular frequency.

Guided waves could be generated through a lot of methods and instruments such as, angle-beam transducers, Inter-digitated circuits (IDC), EMATs, array of elements (strip or annular). There are advantages of each method over the other and their use is based on the need and accessibility of the target specimen. One of the most common methods is the use of a wedge transducer (an angle-wedge transducer). This method of generating waves in an isotropic plate is described by Viktorov [13]. Wedge transducers are optimum for the generation of various guided waves modes and also directing the direction of propagation, unlike the case of a comb transducer or an IDT. The use of comb transducers is also described by Viktorov [13] and is used in this research; it is discussed in more detail in chapter 4.

2.4.3 Phase and Group Velocity Dispersion Curves

Dispersion is a phenomenon where the phase velocity is dependent on its frequency. To better understand the Lamb waves, the dispersion relation and the variance in the phase and group velocities with the frequency is important to study. The phase velocity is the fundamental characteristic of a Lamb wave [13]. With that information, we can determine the wave number and calculate the displacement profile (i.e., wavestructure) at any frequency for any mode. Phase velocity is the speed of an individual wave, while the group velocity is the speed of a travelling group of waves (better known as a wave packet) containing the waves of an identical frequency. As thickness of the plate is what makes these Lamb waves, the phase and group velocities are dependent on a frequency-thickness product and are depicted as dispersion curves. From the foundations of wave propagation in an elastic string, the phase velocity is $c_p = \omega/k$ and the group velocity is $c_g = d\omega/dk$ where ω is the angular frequency $2\pi f$ and k is the wavenumber. There exist three cases (1) $c_p > c_g$, the classical dispersion example where the wave appears to originate behind and travel to the front; (2) $c_p = c_g$, no dispersion as in the case of bulk waves; and (3) $c_p < c_g$, anomalous dispersion, where the wave seems to appear at the front and travel to the rear [1].

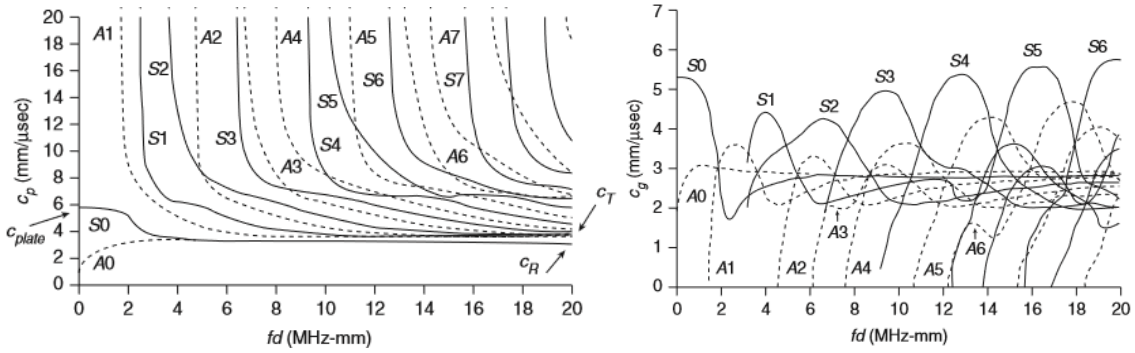

Figure 2.5: Dispersion Curves of phase velocity and group velocity for aluminum as a function of the frequency-thickness product [1]

The lower order modes (A0, A1, S0, S1) are generally easier to generate at a given frequency because the modes are more spread out than at higher frequencies. From the phase velocity dispersion curves, appropriate mode and frequency are chosen for the sensor design. In chapter 4, plates of two different thicknesses are chosen to preferentially excite the S1 mode at the longitudinal wave speed and calculations are performed to compare the group velocity of the travelling wave packet theoretically and experimentally.

Chapter 3 – Processing of Thick Film Transducers

The deposition of inorganic and organic thick films onto plates is described in this chapter along with the other processing steps necessary to make functional ultrasonic transducers.

3.1 Film Transducer Materials

3.1.1 Bismuth Titanate

Piezoelectricity can occur naturally in materials such as Quartz, however polycrystalline materials must be polarized to alter their dipole moments and impart piezoelectricity. Bismuth Titanate $Bi_4Ti_3O_{12}$ (BIT) was first discovered by Aurivillius in 1949. This material has been shown to display ferroelectric properties up to temperature of 670 ^oC, which is significantly higher than PZT (~200 ^oC). Consequently, BIT could be a valuable material for high temperature piezoelectric application, optical exchanging, and capacitors, although its d_{33} is much lower than PZT. $Bi_4Ti_3O_{12}$ ceramics are prepared by a solid-state reaction where it is desiccated at a low temperature followed by sintering at high temperature. Ferroelectric materials such as BIT have found their use in the sensor industry to serve as alternatives for the traditional PZT. Apart from the obvious environmental and health issues related to lead-based materials, it is the evaporation of Lead Oxide (PbO) which is hazardous. PZT is prepared by reaction of individual oxides at high temperatures, among which PbO is one and due to its volatility, it easily enters the atmosphere. PZT can be doped with Bismuth Titanate to counter the disadvantages of PZT. The sol-gel method uses acetic acid and that leads to it reacting to the surface, hence we looked for alternative binder and reagents to overcome this problem. In comparison to other materials, BIT does not oxidize at high temperatures and there is barely any acoustic loss due to this. The sol-gel method has been adopted by many

researchers since the 1990s and it provides excellent synthesizing conditions for BIT films. Bismuth Titanate's *perovskite* lattice structure is also unique, which provides it with some remarkable properties. Perovskite type structures exhibit the same crystal structure as Calcium Titanium Oxide with the oxygen in the edge centers as shown in Figure 3.1 [21]. The perovskite structure results in strong dipole forces and a high d_{33} coefficient allowing them to be used for piezoelectric applications. BiT has a high coercive field of about 40 KV/mm [30] which sometimes makes it difficult to pole; unless inserted in an oil bath to limit breakdown. If a dielectric breakdown occurs, the insulative BIT becomes a conductor and there is a permanent short-circuit through the material rendering it unable to be poled. The relative dielectric constant is the ratio of the permittivity of the material ε over the permittivity of free space ε_o and BIT is said to have a low dielectric constant at 107 [21].

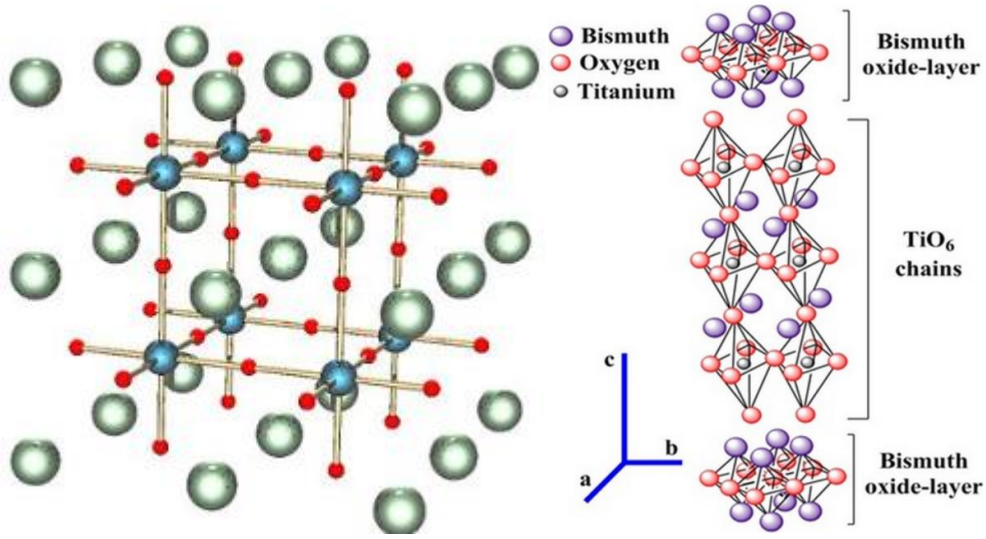

Figure 3.1: Calcium Titanate ($CaTiO_3$) perovskite structure (left) and Bismuth Titanate ($Bi_4Ti_3O_{12}$) which is made up as layers of its components (right). [34]

3.1.2 Lithium Niobate

Lithium Niobate ($LiNbO_3$) is a single crystal material with a high curie temperature of 1150 ^oC. They possess excellent electro-optic, nonlinear optical and piezoelectric properties, hence the single crystals find their use in optical modulators or SAW devices. Even though it has a high curie temperature and has shown to work until about 1000 ^oC, due to oxidization

it often tends to lose oxygen above 600 ^{o}C, causing random unreliable dielectric properties. Due to this reason, the Lithium Niobate films are doped with Barium Titanate. Barium Titanate has a low curie temperature at 120 ^{o}C, however due to its richness in oxygen, the oxidation effect of Lithium Niobate is reduced. It takes shape in the trigonal framework and single area precious stones of viable size have been developed by the Czochralski technique. Lithium Niobate has a lower dielectric constant compared to PZT and BIT which leads to a reduced energy response when in operation. To tackle this problem and to allow it to be used for higher temperatures, work was performed to dope the Lithium Niobate with another material such as Barium Titanate to provide functionality after 600 ^{o}C as the doped material reduces the rate of oxidization of Lithium Niobate. The Barium Titanate also being a ferroelectric provides good acoustical response before it starts to deteriorate at higher temperatures. Another approach adopted was to use a protective Alumina (Aluminum Oxide Al_2O_3) layer on top of the deposited film to further reduce the oxidization effects on its operation.

3.1.3 Organic Bismuth Titanate

Traditionally, organic film coatings have found their use in safeguarding metals against corrosive environments in both academic and industrial settings. Their primary objective is to act as physical barriers for oxygen and water. Use of organic films for piezoelectric applications is relatively new as there are some disadvantages associated with it.

The fabrication of the organic films is very similar to the inorganic films. However, the materials used are different and there are some precautions that need to be followed when dealing with organic materials. An inorganic powder of choice (work has been primarily done with Bismuth Titanate) is mixed with a compound of organic solvents, binders and dispersants. As the organic solvents (mixture of xylenes and ethanol) are heavier in nature than their counterparts (water being the inorganic solvent), the powder tends to agglomerate, so there is a need for a dispersant to mold it into a homogenous mixture. The dispersant used here is of negligible quantity and has no effect on the properties of the film. A step-wise procedure was prepared to properly formulate the transducer.

3.2 Transducer Fabrication

3.2.1 Sample Preparation

For the spray-on transducers to operate, the sample under test has to be ferroelectric in nature to act as the ground electrode. The current interest is in metal test samples. A majority of factory components are made of inert alloys such as stainless steel and aluminum. Even though they have very low conductivity, the presence of even a few free electrons allow the film to experience the electric field for their use for ultrasonic transducers. Many of these metals have protective coatings, such as anti-corrosion, however, that should not pose any challenges for the spray-on transducers.

The properties of a film are strongly dependent on the crystal structure, thickness and its microstructure. A film of higher green density and lower porosity has been shown to work better [9]. The substrate needs to be cleaned from any surface smudges, salts, etc., before the film is deposited. Impurities on the surface could result in poor adhesion or limited sound transmission.

3.2.2 Fabrication Procedure

The Bismuth Titanate powder used was 99.99% pure $Bi_4Ti_3O_{12}$ 200 mesh (75 µm particle size) supplied Lorad Chemical Corporation. Lithium Niobate powder was a 99.99 % pure $LiNbO_3$ 325 mesh (45 µm particle size) supplied by LTS Research Laboratories, Inc. The Barium Titanate used was 99% pure $BaTiO_3$ 325 mesh (45 µm particle size) is supplied by Acros organics.

Kobayashi's pioneering research guided our research at Penn State in terms of the composition, deposition, curing, and results. Most recently was Ledford's work to find an alternative to the sol-gel process, which resulted in a non-organic solvent mixture. Ledford's work with Aremco Ceramabind 643 and 830 binders showed that lithium-silicate based inorganic binders eliminate the need for thermal processing and allow the film to cure at room temperature. Xu's work perfected the fabrication process, resulting in minimal porosity and a film with higher green density. Various tests were performed with different

concentration ratios of the individual materials of the film. Multiple tests resulted in a slurry which was in a powder-binder-water ratio of 1:0.2:0.8 by weight in grams.

To find the best weight ratio concentration of the powder-binder-water, the primary goal was to create a homogenous film with minimum porosity and least cracking. It was important to consider a binding material that has a high temperature rating and good adhesion to various types of surfaces. Ceramic binding agents supplied by Aremco are mostly inorganic in nature and the application dictates the type of agent required. Initial work was done with Ceramabind 643 and 830. Ceramabind 643 is a basic solution compatible with most ceramic and metal powders and it is an excellent binder for high temperature applications as it has a temperature resistance up to 3000 F (1650 ^{o}C). Ceramabind 830 is also a basic solution compatible with most oxide and metal powders and is perfect for films thicker than 100 µm. The temperature rating for Ceramabind 830 is 2000 F (1093 ^{o}C), but it is preferred over Ceramabind 643 as it is non-reactive with all metal surfaces, while Ceramabind 643 is reactive to aluminum and its alloys. Furthermore, Ceramabind 830 can be allowed to cure at room temperature while Ceramabind 643 might need some thermal treatment around 100 ^{o}C to cure.

The Sol-gel composite films have been successful in combining surface adaptability with the piezoelectric properties; however, its fabrication incorporates acetic acid, which can lead to problems such as pyrolysis and long-term corrosion on mild steel pipes. Our research group's focus was to replace the acidic sol-gel solution with a basic lithium-silicate solution. The powder-binder concentration, curing conditions, post processing techniques and workability was studied by Xu and the results used herein. The preparation of the films is a meticulous procedure with the average fabrication time ranging between 1 and 3 hours. As mentioned before, two different films are produced for use in high-temperatures and guided wave propagation. The pressure through the air gun while spraying was set to be 20 psi. Various other pressures were tried but while going to 30 psi or higher it was noticed that the slurry would spread away from the applied location due to higher pressure, while spraying with a lower pressure (15 psi or less) caused the slurry to clog the nozzle. The following steps are optimized for best results.

1. Select the powder (BIT or Lithium Niobate/Barium Titanate) and mix with Ceramabind 830 to achieve a **1:0.2:0.8** ratio (powder-binder-water by weight ratio); a plastic stirrer was used to rigorously mix the powder and binder, but it could be mixed with a ultrasonic horn;
2. Create the solution by combining the mixed powder/binder with distilled water at the specified concentration in a 15 ml glass vial;
3. Prepare the substrate by roughening the surface with a dry 600 grit sandpaper and then clean it with isopropyl alcohol;
4. Spray the slurry onto the substrate with an air gun. The air gun pressure should be 20-22 psi and the nozzle should be approximately 20 cm from the surface. Alternatively, apply slurry with a brush;
5. Dry each layer of the sprayed film in the relatively low humidity environment (15-20%) of a glove box for at least 15 minutes to avoid cracking;
6. Repeat steps 4 and 5 to achieve the desired film thickness (preferably thicker than 120 μm). The average thickness of a single spray is 18 μm;
7. Use a thickness gage to measure the average thickness of the film;
8. After the film layers have cured, brush apply a conductive silver paint (SPI Chemicals Inc) on the portion of the film to become the transducer to a thickness of approximately 30 μm. Each layer takes approximately 15 minutes to cure in the low humidity setting, so if there are 8 spray repetitions, it will take about 2 hours. For films thicker than 8 layers the cure time for a layer may be longer.
9. Once the electrode is applied, heat the sample to 60 °C for a few minutes with a heat gun to allow the electrode to dry. This step is optional as the electrode can air dry in a longer time;
10. Attach a bare Nickle Chrome wire (supplied by Consolidated) with silver paint to serve as the lead wire as shown in Figure 3.2;
11. Pole sample at a desired electric field for at least 20 minutes at ambient temperature (details are given in Section 3.3).

Processing organic BIT films is more challenging than the inorganic films because many safety precautions have to be followed when dealing with the toxic and hazardous substances. The organic compounds used in this preparation are hazardous chemicals and mishandling can lead to other complications. Work by Arunkumar [33] and Morandi [51] provided insight in creating these mixtures. In their work, experiments were performed for Titanium Oxide and it was concluded that a solvent-dispersant combination of Ethonal:Xylenes with a 50:50 volume ratio and 1 wt % blown menhaden fish oil (supplied by The Tape Casting Warehouse, Inc., Grade Z-3) were optimum. The solvents used were Xylenes (Mixed, 97% by Alfa Aesar Inc.) and Ethanol (Anhydrous 99.5%, 200 proof by VWR Chemicals). The slurry was then introduced with a homogenizer, plasticizer and a Binder. The mixture contained a 58.95% solid loading and a high green density. Morandi's [51] work showed that a slurry with the same properties could be prepared without a homogenizer or plasticizer. To apply this method for BIT, a slurry batch for a solid loading of 33% was created. BIT is a heavier and larger powder than Titanium Oxide (in terms of density and powder size used). Due to this a high solid loading presents problems with deposition and subsequent curing. The binder added here was a powdered form of Polyvinyl Buyral (PVB) and it was in a smaller content than the liquid ceramabind 830. This further made the slurry heavier making it only deposable by painting, dipping or tape-casting. The mixture could be inserted in an ultrasonic horn mixer for homogeneity or mixed with a stirring rod. The slurry was then deposited on a cube sample with a paint brush with the maximum possible precision to get a uniformly thick slurry. Similar to the sol-gel method, the organic components need to be evaporated and requires the film to be thermal treated and cured.

Figure 3.2: Bismuth Titanate, Lithium Niobate/Barium Titanate and Organic Bismuth Titanate film transducers (left to right)

3.3 Post Processing and Poling

Once the film is deposited and has cured as prescribed in the previous section, an electric field is applied in order to pole it. The electric field supplied to the film is dependent on its thickness and the coercive field of the film. The purpose here is to realign the dipoles in the material in one direction to create the piezoelectric effect. For BIT the coercive field is around 40 kV/mm, but this has been shown to vary for other conditions, ranging from 35-50 kV/mm [8, 30, 32], while single crystal Lithium Niobate has a coercive field of 22 kV/mm [31] and the addition of Barium Titanate barely alters that value. Coercive field is a measure of the ability of a ferromagnetic material to withstand an electric field without depolarizing.

Poling of BIT and some other ferroelectrics can be challenging as they have a high coercive field but a low dielectric constant. This allows only a narrow band of acceptable electric fields to polarize them before there is a dielectric breakdown. Thus, a silicone-oil bath was used for the BIT films. However, for field applications it is difficult to place the target specimen in an oil-bath, especially if it is part of a bigger system. Poling was instead performed at a lower electric field after the target surface was heated on a hot plate set to 150 ^{o}C, which was shown to give the best acoustical response [9]. This increased the poling time but eliminated the need for an oil-bath poling system altogether.

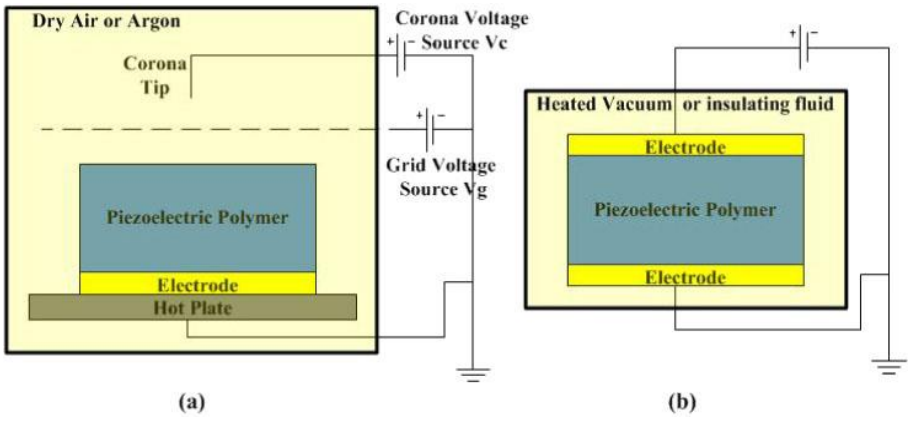

Figure 3.3: Polarization of a piezoelectric element in dry air using a corona tip (a) or in a heated vacuum or oil-bath using a contact DC current (b) [42]

The films here were poled with an ORTEC 556H High Voltage Power Supply. Poling here was performed by contact poling; the top electrode while the substrate acts as the bottom

electrode, as seen in Figure 3.3 (b). However, instead of having the sample in a heated vacuum it is placed on a hot plate in air. Another poling mechanism is through the use of a corona tip (Figure 3.3 (a)), but that was not used for poling in this research. To pole the ceramic, it is important to know the film thickness and the coercive field. A Heidenhain length gauge was used to find the thickness for smaller bulk samples, however for larger structures, the thickness has to be estimated or another instrument may have to be used. From this thickness, an appropriate poling voltage can be obtained: *V = thickness * 40 kV/mm*. Each spray is around 18 µm thick, so a coat of 5 sprays will yield about 90 µm thick film and would require a voltage of 360 Volts to properly pole. Due to the matrix of the film where the particle size of individual components is different, it facilitates some current leakage, much more so than a film of pure BIT. The amount of current can vary wildly depending on thickness and fabrication variations and due to this, the actual poling voltage applied is a lot lower (down to almost half the coercive field). A DC current was applied using the lead wire from the top electrode and the substrate as the ground. After checking for short circuits with a multimeter, voltage is quickly ramped up to roughly half of the coercive field. Subsequently, voltage is manually increased at a gradual rate towards the coercive field. If there is a pop-sound, the breakdown voltage has been reached and the voltage is reduced by about 10 volts and left to pole for at least 20 minutes. The BIT films were poled at 220 volts and the Lithium Niobate films were poled at 160 volts. The organic films being thicker were poled at almost 280 volts. The poling time is dependent on the thickness of the film, porosity and area of the film. Poling could be performed at room temperature as well, but Xu's work showed that poling at higher temperatures lead to a higher remnant polarization and was a faster process.

For the organic films, sintering is required is to cure the films. The process of sintering is defined as the compacting and forming a solid mass of material through the means of heat or pressure, without reaching its liquefaction melting point. Sintering is an important step when using sol-gel mixtures as the acetic acid needs to be evaporated in order for the slurry to adhere on to the surface and so that the powder particles could pack tightly. A highly porous film leads to bad electric properties and the danger of a breakdown. Similar to the sol-gel method, the organic method requires the xylenes to be evaporated as the large atomic structure can induce porosity and trap other non-essential products. The film is placed in a

furnace at about 300 ^{o}C for about an hour or so depending on the film thickness and the area of its application. Xylenes when heated, release benzene in the air which is toxic so the sintering is performed in a fume hood. As the film densifies, trapped air bubbles escape leaving a less porous film compared to the inorganic films. The average thickness of these films was around 250 µm which are almost 100 µmeters thick than the BIT films, where this is brushed on for a layer while the inorganic BIT are sprayed about for about 8 sprays.

A layer of conductive silver paint is applied as an electrode on the film after it has cooled down (about 3-4 hours at least or left overnight). Wires are then attached on to the silver and the films are ready to pole. As these are thicker films than the inorganic films, they require a higher electric field for polarization. Poling for these films were performed on a hot plate at 150 ^{o}C with an electric field of 30 kV/mm for 30 mins. As this generally yields a thicker film consisting of many different chemicals, the poling could take longer than inorganic films, but due to sintering, the film packs very nicely to yield a uniformly polarized film and longer lasting polarization.

3.4 Bulk Wave Results

Once the transducer is prepared, it is imperative to quantify its properties in order for it to classify as a candidate for further testing. The first set of tests performed with the films were pulse echo through the bulk of the material they are deposited on. Films of at least 120 µm average thickness were prepared on N-50 austenitic stainless-steel cubes as shown in Figure 3.2. The cube is 7 mm thick and 25 mm long by 25 mm wide. Through an AP International YE2530A d_{33} meter, the piezoelectric coefficients for both sets of films were measured. Pulse-echo measurements are recorded for thickness measurements of the cube and an A-scan was plotted and Signal-to-Noise ratio was obtained along with the center frequency of the transducer. A National Instruments function generator NI PXI-1042 and a Panametric-NDT 5800 pulser/receiver was setup. Instrument parameters for the thickness measurement are shown in Appendix A.

3.4.1 Pulse-Echo Tests

The through-thickness data from the transducer when exited with a single pulse is shown in Figures 3.4 and 3.5. In the case of BIT films, the first reflection occurs at the 5.38 µs, followed by another reflection at 7.83 µs. As the difference in the two reflections is 2.45 µs, for a 7 mm thick sample, the distance the longitudinal waves have to travel is 14 mm for a pulse-echo setup. This gives us an experimental wave speed of 5.714 mm/µs. Similarly, calculations are performed for the Lithium Niobate films. Here the difference between the first and second reflection was 2.467 µs (7.629 µs – 5.166 µs) and the wave speed measured was 5.67 mm/µs. The calculated longitudinal wave speed for both the films is very close to universally accepted longitudinal wave speed of 5.79 mm/µs for stainless steel.

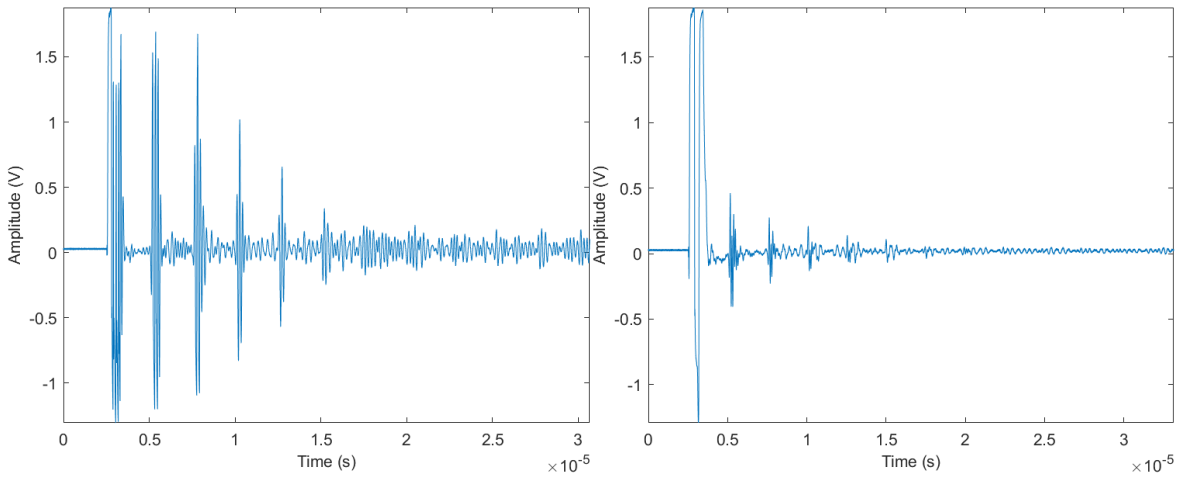

Figure 3.4: Pulse-echo A-scans for the BIT (left) and Lithium Niobate/Barium Titanate (right) films

The Piezoelectric coefficient is also measured for the films however, the meter is designed for free standing films, while these are films attached to a substrate. This makes the measurements less reliable and far from the single crystal (or film) d_{33} values. The recorded coefficient values for BIT was 11 pC/N and Lithium Niobate was 4 pC/N.

Pulse-echo measurements for the organic films were also recorded through the thickness of the substrate. As is seen in Figure 3.5, the signals are clean and the first reflection occurs at the 5.167 µs, followed by another reflection at 7.585 µs in the case of the BIT films. As the

difference in the two reflections is 2.418 µs, and for a wave to travel 14 mm through the thickness of the specimen, it must have a longitudinal speed of 5.789 mm/µs, which is exactly the referenced wave speed in stainless steel.

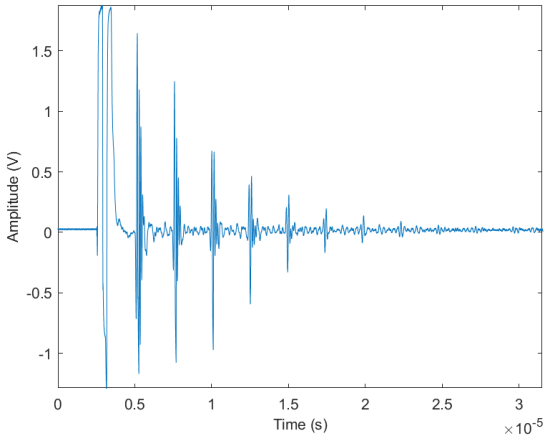

Figure 3.5: Pulse-echo A-scans for the Organic Bismuth Titanate films

3.4.2 Signal-To-Noise Ratio

Signal-to-noise ratio (SNR) is calculated by taking the ratio of the rms value of the amplitude (peak-to-peak) within the mode window to the rms value of the noise window in decibel units giving by this formula.

$$SNR = 20 * log_{10}\left(\frac{V_{pk-to-pk}}{V_{noise}}\right)$$

The rms value is calculated by multiplying $1/(2\sqrt{2})$ to the peak-to-peak voltage. The signal to Noise Ratio along with the Signal strength for the three films is shown in Table 3.1.

Table 3.1: Signal-to-Noise calculations for the Inorganic and Organic films

Film	*BIT*	*LiN/BaTi*	*Organic BIT*
Signal Window (µs)	5.071 – 5.739	5.071 – 5.554	5.030 – 5.635
Noise Window (µs)	5.756 – 7.510	5.615 – 7.490	5.675 – 7.450
Signal Strength pk-pk (V)	2.895	0.868	2.815
Noise Strength pk-pk (V)	0.267	0.156	0.284
Signal rms (V)	1.024	0.307	0.996

Noise rms (V)	0.094	0.055	0.100
Signal Strength (dB)	9.321	-1.232	8.990
Noise Strength (dB)	-11.484	-16.157	-10.939
Signal-to-Noise Ratio (dB)	20.716	14.926	19.929

3.4.3 Capacitance

Capacitance readings were taken for the three films shown in Figure 3.2 with a Keysight U1733C Handheld LCR Meter. Measurements for the films were recorded for five different frequencies as shown in Table 3.2.

Table 3.2: Capacitance values in pF for the three films at various frequencies

Frequency (kHz)	*BIT (pF)*	*LiN (pF)*	*Organic BIT (pF)*
0.1	1773	1930	163
0.12	1678	1170	162
1	1040	802	160
10	709	396	157
100	550	248	153

The free relative dielectric constant is calculated for capacitance at 1 kHz, where the dielectric constant (k) is $(C * t)/(A * \varepsilon_o)$ where C is the capacitance, t is the film thickness, A is the area of the electrode and ε_o is the permittivity of free space = $8.85 * 10^{-12}$ C^2/Jm. The dielectric constant is the ability of a material to store charge. The parameters used to find the dielectric constant is shown in Table 3.3

Table 3.3: Parameters of the three films to calculate the dielectric constant

Material	*Film Thickness (μm)*	*Electrode Area (m^2)*	*Capacitance (pF)*
BIT	178	$138 * 10^{-6}$	1040
LiN	222	$152 * 10^{-6}$	802
Organic BIT	224	$28 * 10^{-6}$	160

The calculated dielectric constant for the BIT, LiN and Organic BIT films are 100.48, 132.36 and 144.53 respectively

3.4.4 Temperature Testing

The Curie temperature of Bismuth Titanate and Lithium Niobate make them ideal candidates for high-temperature testing. These films were inserted in the tube furnace and peak-to-peak voltage measurements for the first and second reflection were recorded. The furnace was set to increase the temperature of the films at a rate of about 5 ^{o}C/min. The Bismuth Titanate films were tested to a temperature of 650 ^{o}C, while the Lithium Niobate films were tested to a temperature of 900 ^{o}C. The first and second echoes were recorded in terms of the signal amplitude and plotted in relation with the temperature ramp seen here in Figure 3.6.

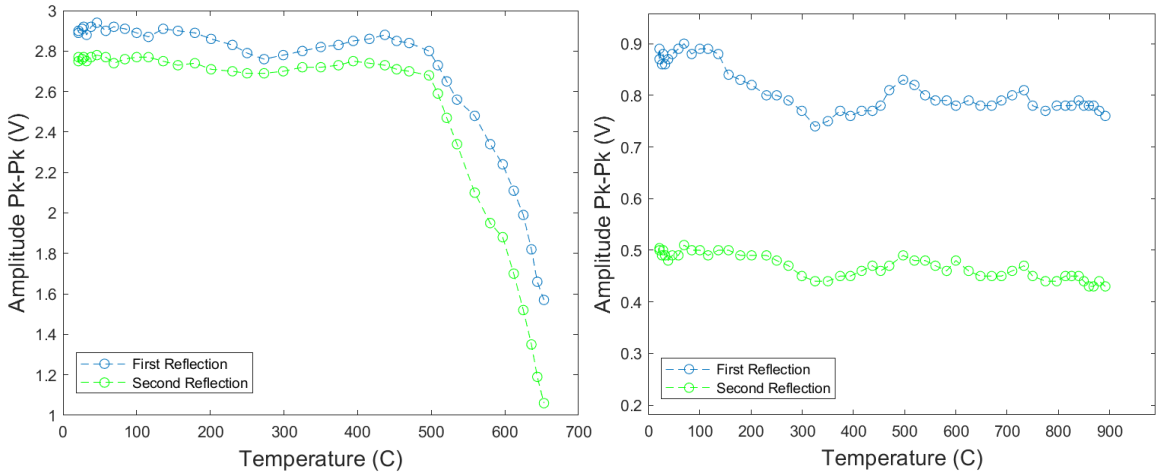

Figure 3.6: Signal amplitude (peak-to-peak) for the first two reflection as a function of the temperature for BIT (left) and LiN (right) films

A Temperature cycling experiment was conducted on the Bismuth Titanate sample where it showed that, when measured during the cooling process, there is minimal loss in the signal strength. The effects of continuous thermal cycling (room temperature-high temperature-room temperature) for multiple times is yet to be studied, however, the result for a single temperature cycle is shown in Figure 3.7 As Bismuth Titanate starts losing its piezoelectricity after 480 ^{o}C, the maximum temperature was 350 ^{o}C to increase the chances of having an operational transducer during the cool down segment. For the single

temperature cycle, temperature inside the furnace was increased at a rate of about 5 ^{o}C/min until 350 ^{o}C, after which it was allowed to cool by itself to room temperature.

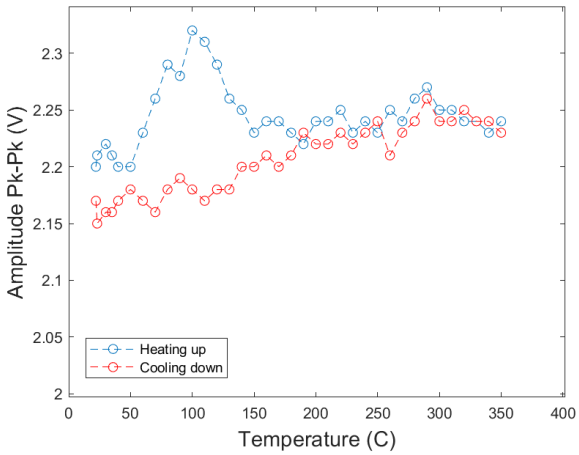

Figure 3.7: Recorded peak-to-peak amplitude of the first echo for a BIT film when subjected to a temperature cycle

3.5 Discussion and Conclusions

Piezoceramic films were prepared using the spray-on method to create ultrasonic transducers. The inorganic films are easy to produce and extremely inexpensive, as the films use very small quantities. A batch of 5 g powder with another 5 g of the solvents is enough to coat at least two of the stainless cubes used for the pulse-echo measurements. For spraying films on bigger areas, the slurry quantity would also have to be increased, but compared to the cost of commercial sensors these transducers are affordable. The respective SNR of 20.72 dB, 14.93 dB and 19.93 dB for the BIT, LiN and Organic BiT films is comparable to commercial transducers. According to the study done by Kobayashi, the films on the planar surfaces yielded an SNR of 16 dB and a center frequency of 3.6 MHz, where the BIT was doped with PZT. Here, without a strong piezoelectric material like PZT, the signal strength is quite strong. With the premise of a working transducer, the films were then subjected to temperature testing. From the capacitance, other parameters to characterize the films could be calculated such as the dielectric constant, dielectric loss, amount of charge in the film and even piezoelectric constant after some analysis. The higher the dielectric constant, more charge could be held by it and used as electric potential. Poling these films requires patience and uniform film thickness. Through some further study, it was found that an Aluminum

Oxide layer was serving as an electrical blanket, which prevented the charges from jumping and short circuiting the film. With the alumina layer, the films could be poled at voltages only a few hundred volts below the coercive field. But it was observed that it also attenuated the noise along with the signal and was hence not used for when testing with plates in Chapter 4.

The peak-to-peak values for the first and second echoes were measured for a temperature excursion. As the Curie temperature of Bismuth Titanate is 670 ^{o}C, it is seen that the transducer begins to degrade around that range. The Lithium Niobate has a higher Curie temperature at 1150 ^{o}C but the experiment could be only performed up to 900 ^{o}C as the conductive silver paint used for the top electrode starts to soften (melting point of silver is 960 ^{o}C) and throw the readings askew. Nonetheless, both inorganic films have the capability to perform at temperatures much higher than PZT or PVDF. As the major focus for this research is on the Bismuth Titanate films, a temperature cycle was performed to show measurements during cooling back down to room temperature. It was observed that despite a temperature cycle, the loss in signal strength is very low and the transducer could be used for further testing. The effects of multiple cycles and other harsh conditions is yet to be performed, but the next chapter is focused on using the film to create a comb transducer to generate ultrasonic guided waves in a plate.

Chapter 4 – Lamb Wave Generation and Reception

4.1 Overview of a Comb Transducer

With the fundamental understanding of ultrasonic guided waves provided in chapter 2, the principle is then applied to various waveguide shapes and materials. There are multiple guided wave modes at a prescribed frequency that could be used for purposes such as damage detection and wall thinning measurements. As mentioned earlier, there are a few ways guided waves could be generated for propagation in a solid. The comb transducer design first suggested by Viktorov [13] and further studied by Ditri and Rose [49] and others depicted a multiple element array (comb arrangement) based on various configurations of element size, spacing and pulsing conditions to generate required modes and frequencies. Comb transducers can produce surface and guided wave in any structure or material as well as very low velocity composite materials where an angle-beam transducer is impossible to use [28]. A comb transducer typically has the following parameters: Element width *S*, number of elements *N* and element gap *W*. The plate thickness is *d*, central excitation frequency of the transducer is f_o and the bandwidth is β. A typical design consists of several strips or rings of electrodes on a piezoelectric material. When a voltage is applied to these electrodes, they generate guided waves of the wavelength corresponding to the electrode spacing [13]. The comb transducers fabricated in this work have W=S, thus the wavelength is equal to W+S.

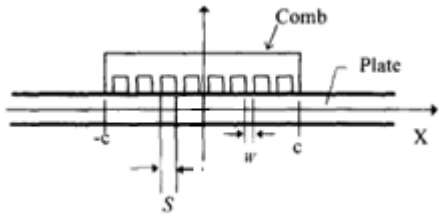

Figure 4.1: A typical comb transducer design on a plate for guided wave generation [48]

The transducers are moved to various distances apart and then velocity calculations are performed. As the spray-on transducer are fixed at a position, they are impossible for that purpose, unless the receiver transducers are sprayed at different distances. When exciting a particular mode, the comb transducer will generate other modes, however, with the use of more elements, the amplitude of the preferential mode could be focused and the frequency distribution narrowed [50]. Comb transducers can be small in design and can be mounted on places difficult to access in service. They can also be used for multi-mode inspection and, based on the material, even used for high-temperatures.

4.2 Comb Transducer Deposition on Flat Plates

A comb transducer arrangement is one of the most fundamental approaches for guided wave excitation. The purpose here is simply to show that the BIT film transducers can function to send and receive Lamb waves in plates, and to compare their results with PVDF transducers.. Aluminum plates were chosen as waveguides for comb transducer deposition. A pitch-catch setup consisting of two sets of comb transducers, working as a pair of actuating-receiving signals, seemed to provide reasonable results. For each waveguide, two sets of transducers consisting a minimum of three elements are deposited to generate the desired S1 mode. The phase velocity and group velocity versus frequency dispersion curves were plotted using the GWIP code created by Jason Philtron at the Penn State Ultrasonics lab. As the excited modes are of lower frequencies, for simplicity, the dispersion curves were only plotted up to a frequency of 1.5 MHz, while the group and phase velocities were plotted up to 10 mm/μs on the vertical axis. The first two modes (A0 and S0) were plotted as 201 points, while the later (A1 and S1) were plotted using lesser points due to their cutoff frequencies. The longitudinal and shear waves for aluminum are taken to be 6.3 and 3.1 mm/μs respectively, the mass density is 2.7 g/cm^3, and thicknesses of 3.2 and 6.4 mm were analyzed.

A propagating mode can be generated where its dispersion curve intersects the activation line for a comb transducer, which is given by the fundamental equation $C_p = \lambda f$. Based on the dispersion curves, excitation frequency and wavelength are determined for the S1 mode. The wavelength is used to determine the element spacing for the comb transducer, while the

group velocity can be used to calculate the time of flight for the mode. The dispersion curves are a function of the material and the plate thickness, which directly affects the element spacing.

Plate 1: Aluminum 3.2 mm Plate

The first experiment was conducted on a 3.2 mm thick aluminum plate 330 mm long by 305 mm wide. The plate was cleaned with a fine sandpaper and then with ethanol and acetone to get rid of any surface smudges or oils. The wavelength of the mode is plotted as the excitation line on the dispersion curve as seen in Figure 4.2. From the dispersion curve, we can find the fastest arriving group and phase velocity of the S1 mode. In this case, the C_p is 6.34 mm/µs and a C_g of 4.19 mm/µs. The excitation frequency is set to be 1.1 MHz and the λ is 5.76 mm, which dictates the ideal spacing for the comb transducer to be 2.88 mm. As this is hand fabricated, a tape mask is created for the film deposition. On this plate, the distance between the actuator and the receiver is 140 mm, while each element is 80 mm wide and the element spacing is 2.8 mm. The film was sprayed on an area of 5130 mm^2 (90 x 57 mm) on two places on the top of the plate. Three elements were applied on each set of transducers, however during the test only one element was used for receiving as shown in Figure 4.3.

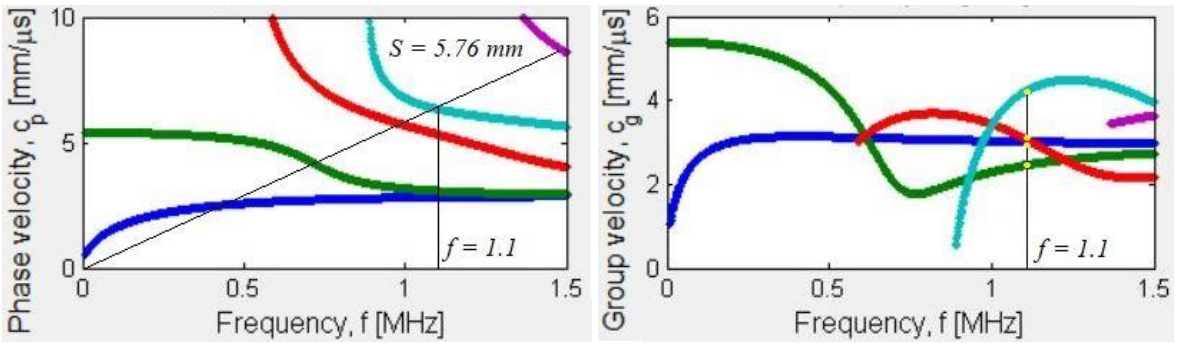

Figure 4.2: Dispersion curves for a 3.2 mm thick aluminum plate showing the activation line on the phase velocity and corresponding group velocities at that frequency

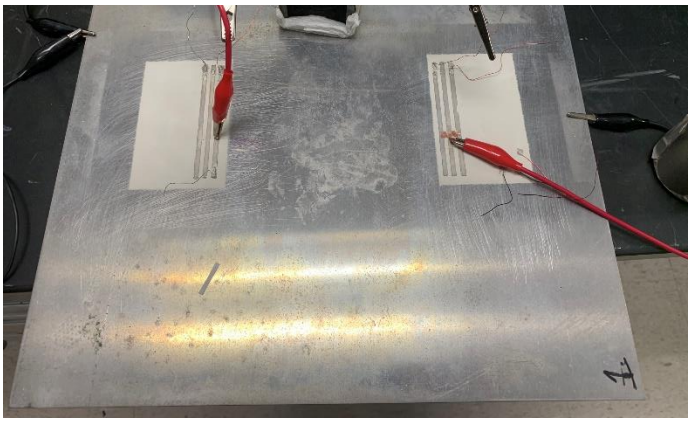

Figure 4.3: A 3.2 mm thick aluminum plate using 3 actuating elements

Plate 2: Aluminum 3.2 mm Plate

The next plate tested was also an aluminum plate of 3.2 mm thickness and 330 mm long by 227 mm wide. The sample was cleaned and two sets of transducers were deposited. The dispersion curves in Figure 4.2 apply here too. Here again for the S1 mode, the C_p is 6.34 mm/µs and a C_g of 4.19 mm/µs. The excitation central frequency is set to 1.1 MHz and the λ is 5.76 mm. The first elements of the actuator and the receiver combs are 160 mm apart and each element is 48.5 mm wide with an element spacing of 2.85 mm. The film was sprayed in an area of 870 mm^2 (50 x 17.4 mm) on either side of the plate. Two elements were applied on each set of transducers, and again only one was used for receiving as shown in Figure 4.4 below.

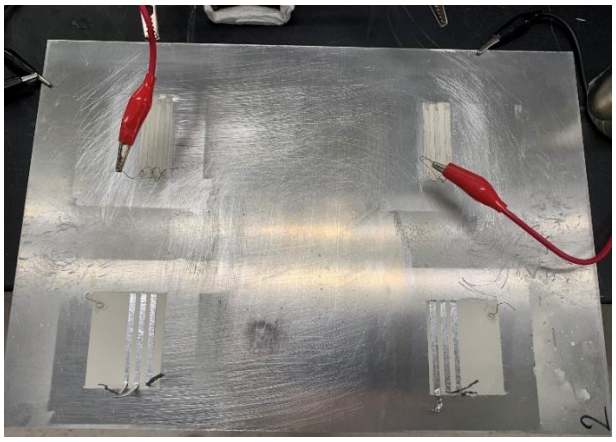

Figure 4.4: A 3.2 mm thick aluminum plate using only 2 actuating elements (wire connected)

Plate 3: Aluminum 6.35 mm Plate

It was important to look at the S1 generated mode in a thicker plate, and an aluminum plate 6.4 mm thick and 305 mm long by 304 mm wide was selected. Dispersion curves are plotted again for this new thickness and shown in Figure 4.5. For the S1 mode, the C_p is 6.01 mm/µs and a C_g of 4.48 mm/µs. The excitation frequency is set to be 0.63 MHz and λ is 9.52 mm. Two sets of configurations (shown in Figure 4.6) were sprayed where one used four elements for actuating, while the other used five elements. The first elements of the actuator and the receiver combs are 135 mm and 186 mm apart for the respective configurations. Each element is 77.5 mm wide with an element spacing of 5 mm, corresponding approximately to half of the wavelength for the excited mode. Unlike the previous cases, the film was sprayed by using a mask in order to have spacing between the film for each electrode. An overall area of 870 mm^2 (50 x 17.4 mm) was applied on either side of the plate.

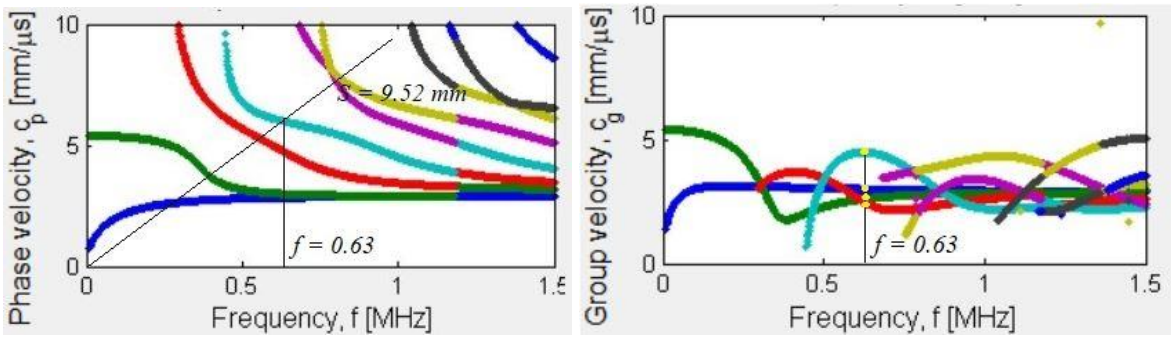

Figure 4.5: Dispersion curves for a 6.4 mm thick aluminum plate showing the activation line on the phase velocity and corresponding group velocities at that frequency

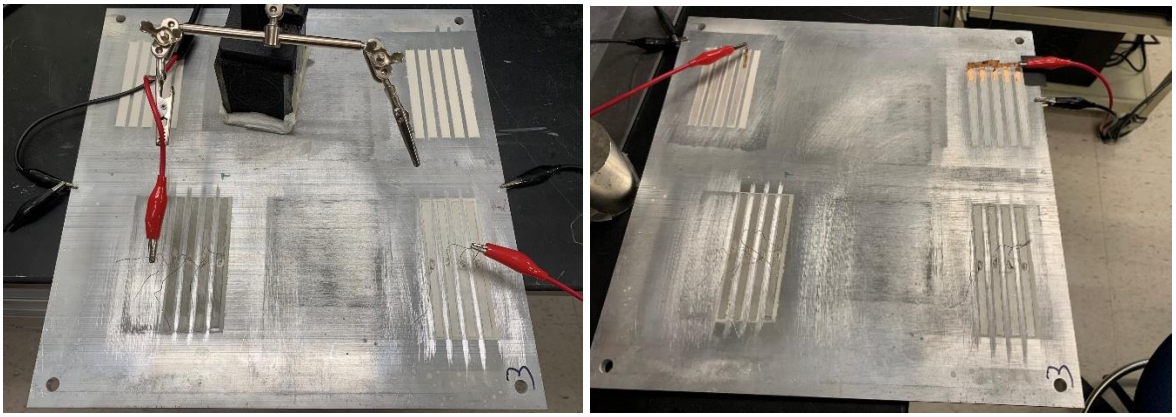

Figure 4.6: Two sets of configurations on plate 3, using 4 elements on the left and 5 on the right

Aluminum 3.2 mm Dogbone Plate

The aluminum dogbone plate has previously-deposited PVDF film transducers as shown in Figure 4.7. This plate was used by H. Cho [7] for his research and was one of the many transducers he had prepared. The dogdone plate is 586 mm long and the center section is 48 mm wide. For the preferential S1 mode, the C_p is 6.34 mm/μs and a C_g of 4.19 mm/μs. The excitation frequency is set to be 1.1 MHz and the λ is 5.76 mm. The first elements of the actuator and the receiver combs are 259 mm apart and each element is 2.7 mm wide with a gap between elements of 2.7 mm. Five elements were applied on the actuating side while only one was used for receiving.

Figure 4.7: The 3.2 mm thick aluminum dogbone sample with PVDF using 5 actuating elements

4.3 Instrumentation and Data Acquisition

The DAQ system used to collect the waveform for the transducers was setup by Cho to perform non-linear measurements with PVDF. A similar setup is created to test the aluminum plates as shown in Figure 4.8. The RITEC 5000-SNAP system, used for the study of nonlinear acoustic phenomena (SNAP) is incorporated here to generate the guided wave modes. All its controllable functions are programmed on a desktop computer and the required interface card and software. The SNAP system is excellent for the use for ultrasonic nondestructive testing as it can make measurements using RF bursts, high power excitations, modular approach as set by the user, signal receiving and processing. This ability to generate

and excite signals through the integration of a software, make this a very useful research tool for ultrasonic measurements.

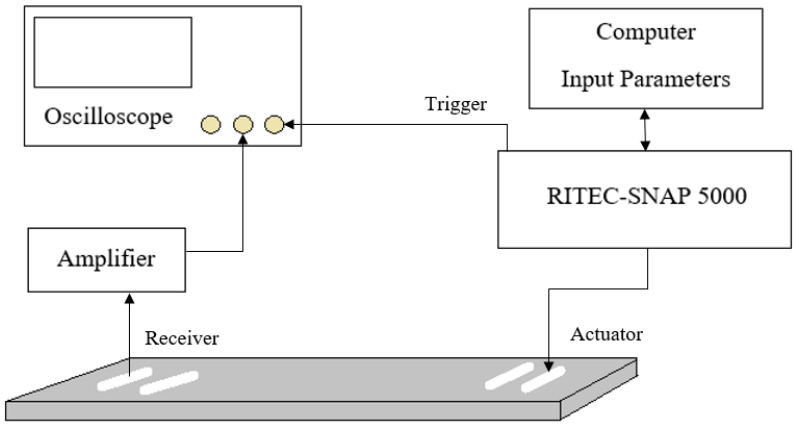

Figure 4.8: Schematic of the guided wave testing setup. A high voltage tone-burst activates the actuator and a low power trigger is used to precisely determine the time at which the transmitter generates guided waves

For the generation of the guided wave mode, frequency is the most important information to have. The excitation frequency calculated from the dispersion curves and other parameters (shown in Table 4.1) of the software are inputted as necessary to the RITEC software and to obtain the best possible waveforms. From this, the SNAP system sends RF tone burst into the actuating transducers. The receiving transducer then sends the electrical signal through an Olympus 5660B pre-amplifier to a Tektronix MSO 2014 oscilloscope with a 1 GHz sampling rate. This amplified signal is fed into Channel 3, while a trigger from the SNAP system is setup on Channel 4 of the oscilloscope. A screenshot of the RITEC software is shown in Figure 4.9 while the functions of each connection and parameter are listed in Appendix B. The waveforms are averaged and then written to a portable USB drive for further analysis. The oscilloscope and the actuating-receiving set of transducers are grounded with the plate, while the core of the coaxial cables is connected to the SNAP system and the receiving pre-amplifier.

Some input parameters stay constant irrespective of the plate thickness and geometry and some are variable as shown in Table 4.1. All the tests are performed in through-transmission with a tone-burst width of 15 cycles. The averaged data come from 512 waveforms, which were modulated using a Hanning window with a DC offset control of 0.75 volts. There are

100000 points in each A-scan, representing an approximate time range of 200 µs. No receiver gain was applied for the PVDF dogbone sample as it was already excited at a very high voltage, however, the BIT transducers are unable to withstand that high of a voltage, and hence are excited at a lower output level and amplified at the receiving end.

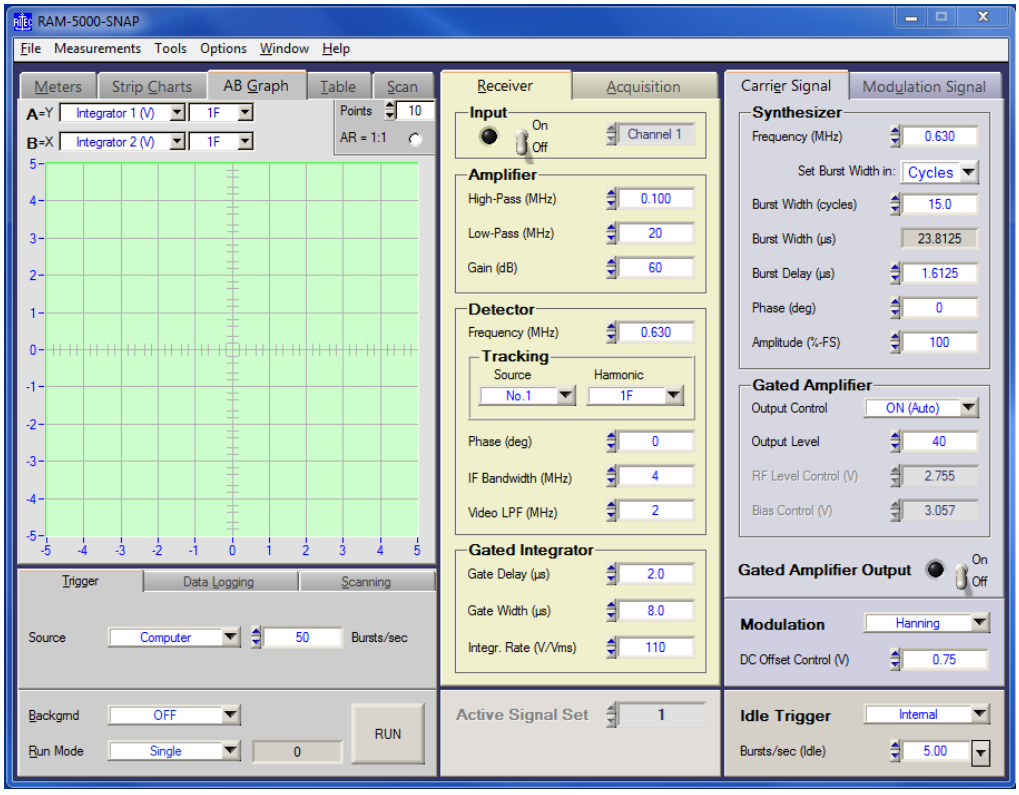

Figure 4.9: Screen-capture of the RITEC software where all the wave parameters are fed

Table 4.1: Variable SNAP settings used for the excitation of guided waves

Input Parameters	*Plate 1*	*Plate 2*	*Plate 3*	*Dogbone*
Excitation Elements	3	2	5	5
Pulse Voltage (Vpp)	440	440	580	1150
Excitation Freq (MHz)	1.10	1.10	0.63	1.10
Time Range (µs)	200.4	200.48	200.2	200
Sample Rate (MHz)	499	498.8	499.5	500
Pre-Amp Gain (dB)	40	40	40	0

4.4 Results and Discussion

A tone-burst of 15 cycles was generated at a particular frequency (depending on the thickness of the plate used). The primary mode under study here was S1, however, other modes are also generated at the same frequency travelling at different velocities. In practice, the activation line actually generates the modes in a region near it giving rise to more complexity in mode characterization.

Table 4.2: Phase and group velocity of the first four modes for a 3.2 mm thick aluminum plate from the dispersion curves

Mode	C_p *(mm/µs)*	C_g *(mm/µs)*
S0	3.08	2.45
S1	6.34	4.20
A0	2.82	3.02
A1	5.33	3.09

Table 4.3: Phase and group velocity of the first four modes for a 6.4 mm thick aluminum plate from the dispersion curves

Mode	C_p *(mm/µs)*	C_g *(mm/µs)*
S0	2.99	2.61
S1	6.00	4.48
A0	2.84	2.99
A1	4.76	2.45

A-scans were plotted in MATLAB from the saved data. Signal-to-Noise ratio of each mode is calculated by using the end-points of the mode and the initial noise.

Plate 1

A tone burst of 15 cycle width was applied to the actuator containing 3 elements in the comb design, which is then received by a single receiving element. After taking readings from one element, an element farther away is used for receiving.

Table 4.4: Predicted Time-of-Arrival for initial modes for Plate 1 when actuating with three elements and receiving with three elements

TOA prediction (μs)	*1st element*	*2nd element*	*3rd element*
S0	60.16	62.45	64.73
S1	35.18	36.52	37.85
A0	48.85	50.71	52.57
A1	47.63	49.43	51.24
Distance from actuator (mm)	147.4	153	158.6

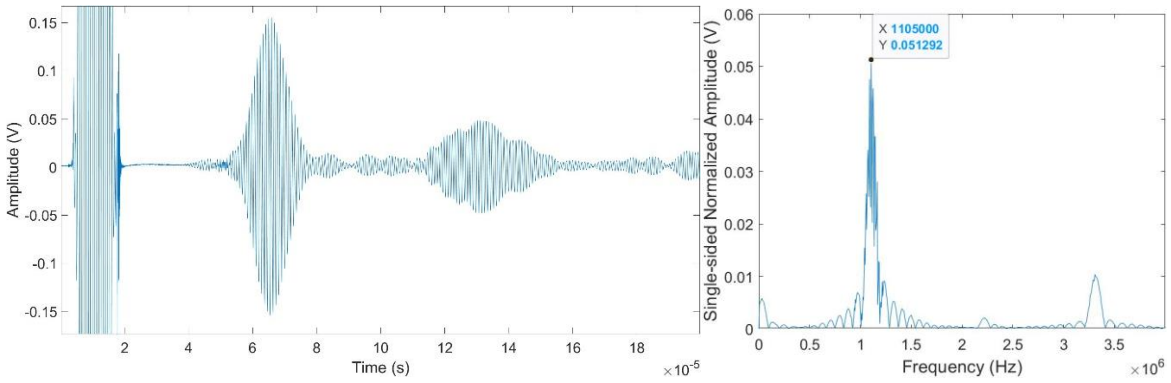

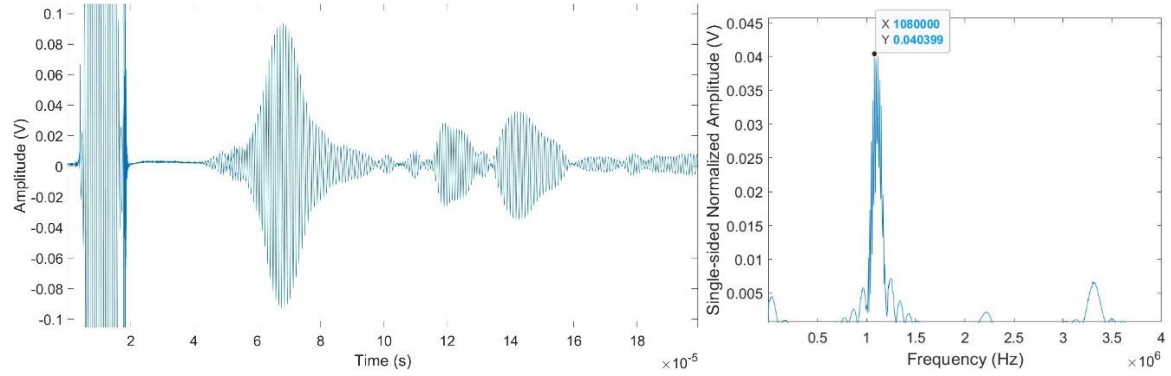

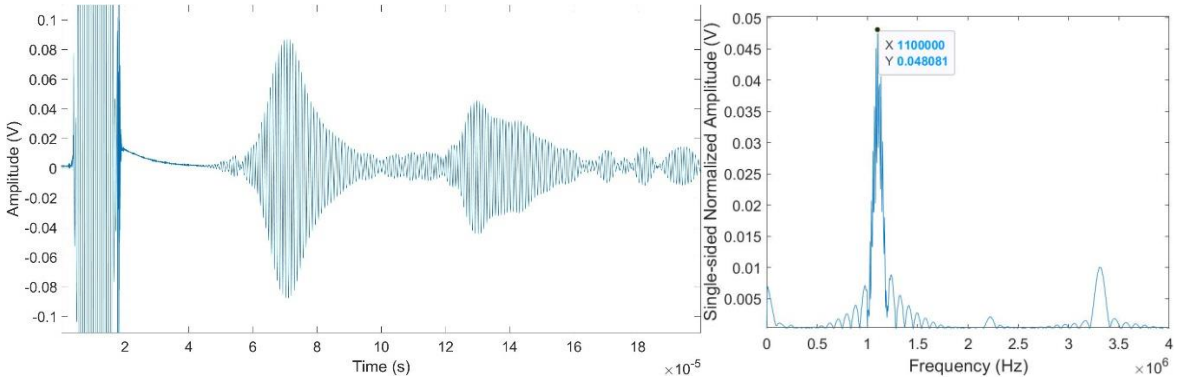

Figure 4.10: A-scans and FFTs of the received signals from the first, second and third elements in the receiving transducer

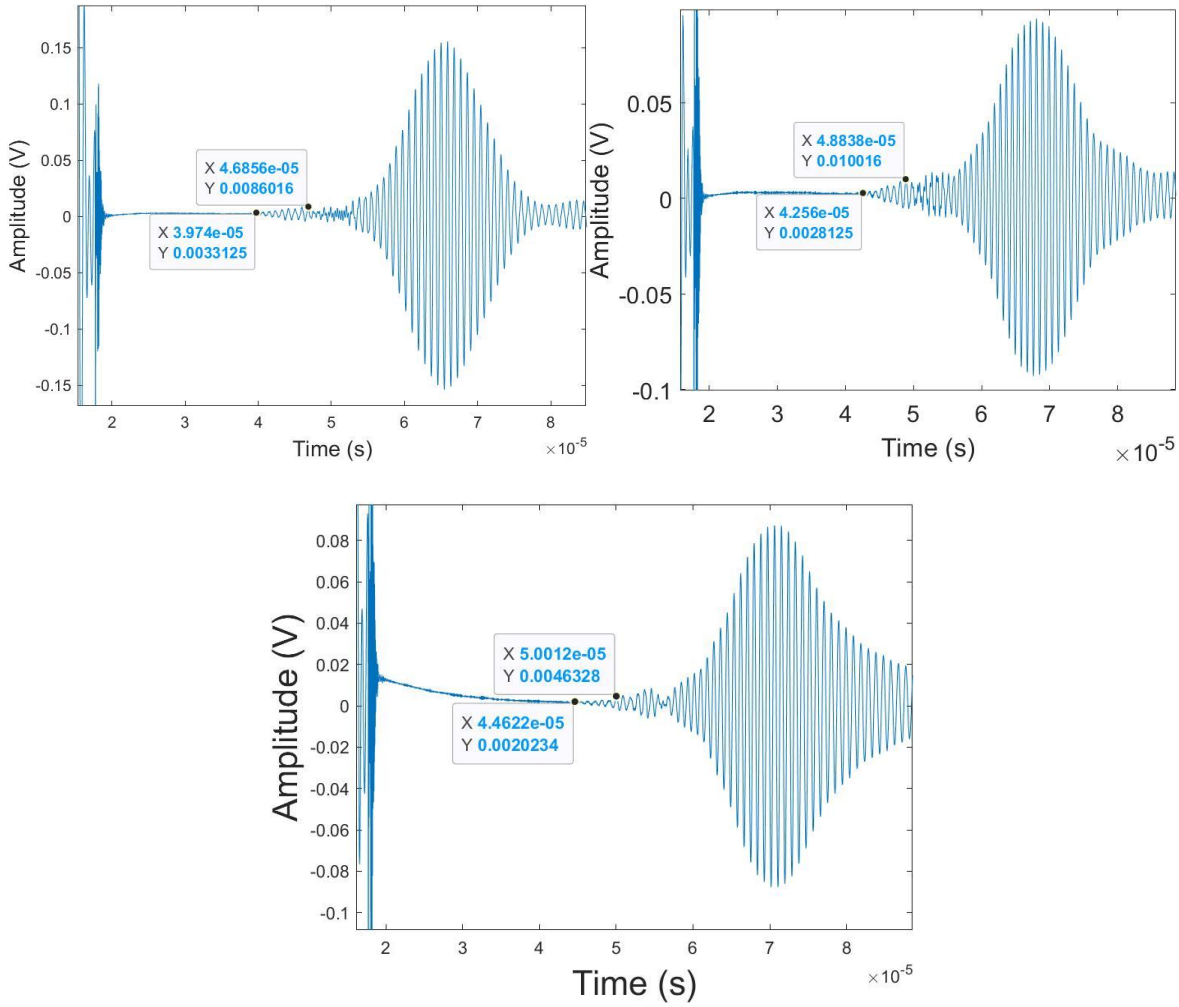

Figure 4.11: The arrival and peak times of the S1 mode packet for the 1st, 2nd and 3rd receiving elements

The received A-scans in Figure 4.10 show the guided wave modes, while the modes arrive around 40 μs, the initial electromagnetic interference prior to 20 μs is not related to the ultrasonic waves. As seen from the waveforms, when received with a farther element, the waves have a longer travel time. Multiple modes are observed; S1 mode has the largest group velocity so it appears first; its amplitude is very small compared to the later arriving A1 mode, which is much easier to generate from a single-sided comb transducer. The frequency spectra are dominated by the excitation frequency (1.1 MHz for all the elements), but some energy at the second and third harmonics is also observed in the FFT plots for each received element in Figure 4.10. Figure 4.11 show the received signal from the three elements where the arrival times and peak times of the S1 mode are marked. The predicted arrival time for the S1 mode is 35.18 μs as shown in Table 4.4, while the arrival of the first mode from this plate was 39.75 μs. The arrival time of the first mode on the third element is 44.62 μs. The distance between the first and third element is 11.2 mm so based on the time difference and the distance, C_g is calculated to be 2.29 mm/μs which is error of 45.2 % from the theoretical group velocity shown in Table 4.2. If the difference between the peak times of the supposed S1 mode is 3.16 μs (50.01 μs – 46.85 μs), the calculated C_g from this is 3.54 mm/μs, which is an error of 15.6 % from the theoretical C_g of 4.2 mm/μs. This delay in the arrival time could be accounted due to the heavy interference in the start of the waveform. Furthermore, a burst width of 15 cycles applied for the tone burst but there is a delay of 1.613 μs from the SNAP system. The waveforms in Figure 4.11 indicate the presence of multiple modes that arrive after the S1 mode, but they are closely grouped in one wave packet and no further analysis is attempted.

Plate 2

On this plate, the comb transducer was designed to replicate the dimensions of the electrodes used in the PVDF samples by Cho [7]. A tone burst of 15 cycles was applied to the actuator containing only 2 elements in the comb design, which is then received by a single receiving element. After taking readings from one element, the waves were recorded using the second element.

Table 4.5: Predicted Time-of-Arrival for initial modes for Plate 2 when actuating with two elements and receiving with two elements

TOA prediction (μs)	*1st element*	*2nd element*
S0	67.63	69.96
S1	39.55	40.91
A0	54.92	56.81
A1	53.54	55.38
Distance from actuator (mm)	165.7	171.4

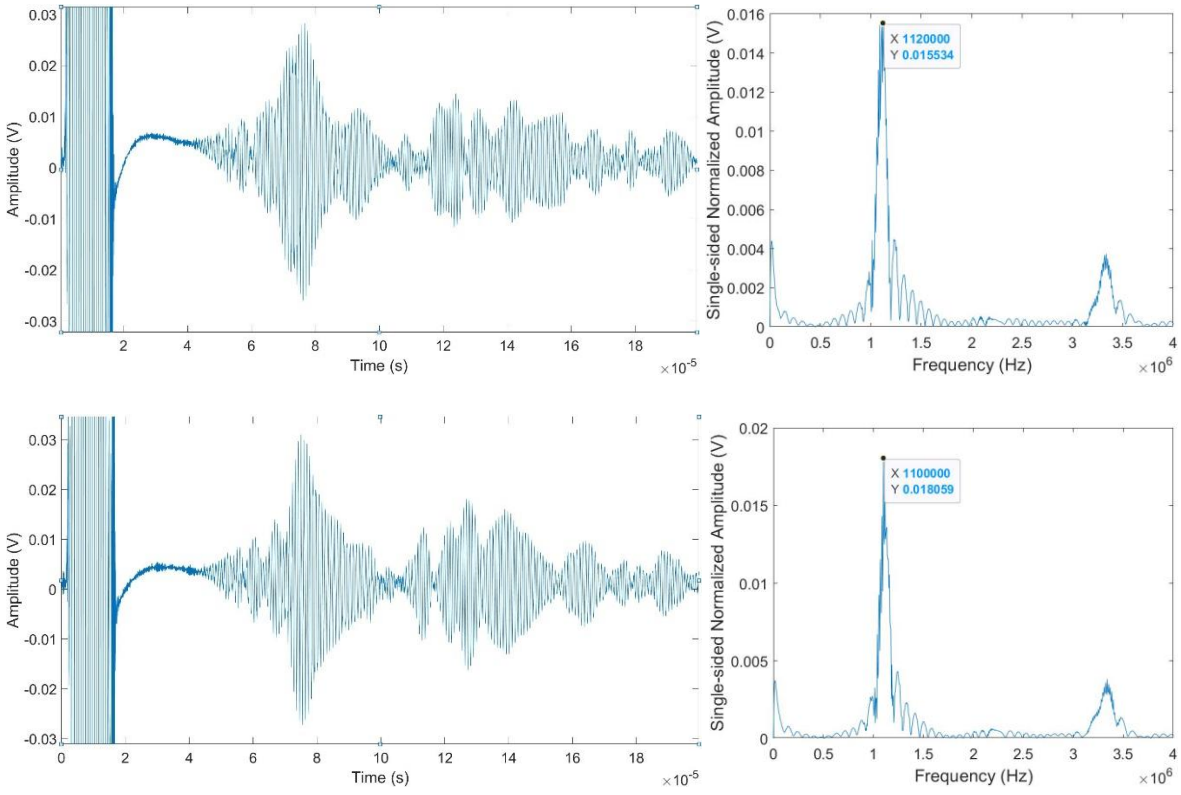

Figure 4.12: A-scans and FFTs of the received signals from the first and second elements in the receiving transducer

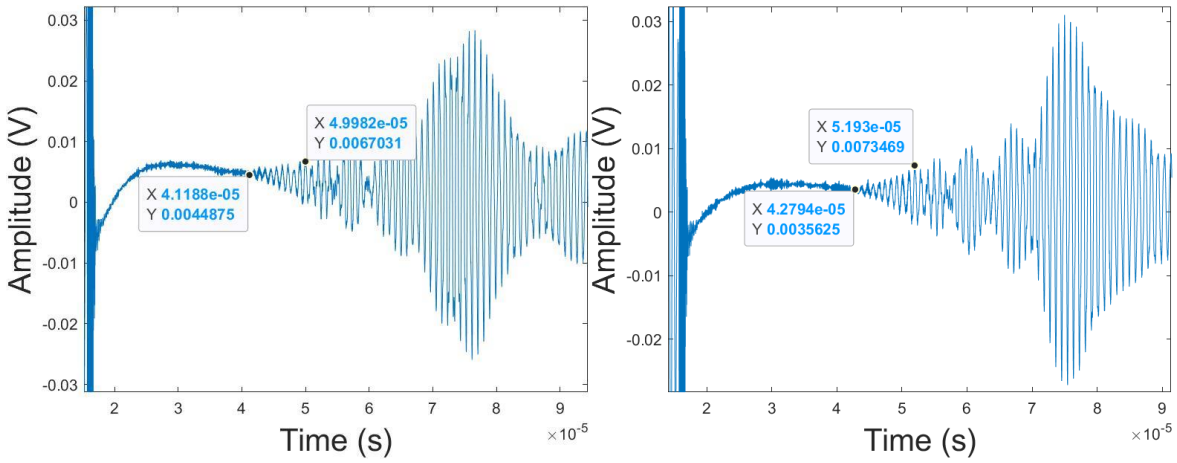

Figure 4.13: The arrival and peak times of the S1 mode packet for 1st and 2nd receiving elements

The received A-scans in Figure 4.12 show the guided wave modes first arriving after 40 µs, and the initial electromagnetic interference is present prior to 20 µs. Again, it is seen from the full waveforms, when received with a farther element, the modes have a longer travel time. The frequency spectra shown in Figure 4.12 confirm that the wave excitation has a frequency of 1.1 MHz for all the elements. The predicted value for the S1 mode is 39.55 µs as calculated in Table 4.5, while the arrival of the first mode from this plate was 41.30 µs and the arrival time of the first mode on the second element was 42.78 µs as shown in Figure 4.13. This is true with the predicted values as despite the delay, the difference between the two arrival times experimentally is the same theoretically. The difference between the arrival times of the supposed S1 mode is 1.48 µs (42.78 µs – 41.30 µs) and for a distance of 5.7 mm between the two elements, the C_g is 3.56 mm/µs. This equals to a 15 error % from the theoretical C_g for the S1 mode in Table 4.2 This error is accounted due to the shorter travel distance and the use of only two elements for actuating, which further causes the waveforms to not look alike for a few later modes. As only two elements were used to generate the waves, it is seen that the modes are even more dispersive (Figure 4.12) than when generated using more elements (Figure 4.10). As S1 is the mode of interest here, and the later modes being grouped together, no analysis for later modes was performed.

Plate 3 (configuration 1)

To show that these transducers work for thicker plates, two different configurations were used. On the first one, four actuating elements were used and four different elements for receiving. A tone burst was applied and readings from each element were noted.

Table 4.6: Predicted Time-of-Arrival for initial modes for the first configuration of Plate 3 when actuating with four elements and receiving with four one elements

TOA prediction (μs)	*1st element*	*2nd element*	*3rd element*	*4th element*
S0	59.34	63.17	66.99	70.88
S1	34.59	36.83	39.06	41.29
A0	51.75	55.09	58.43	61.77
A1	63.39	67.48	71.57	75.66
Distance from actuator (mm)	155	165	175	185

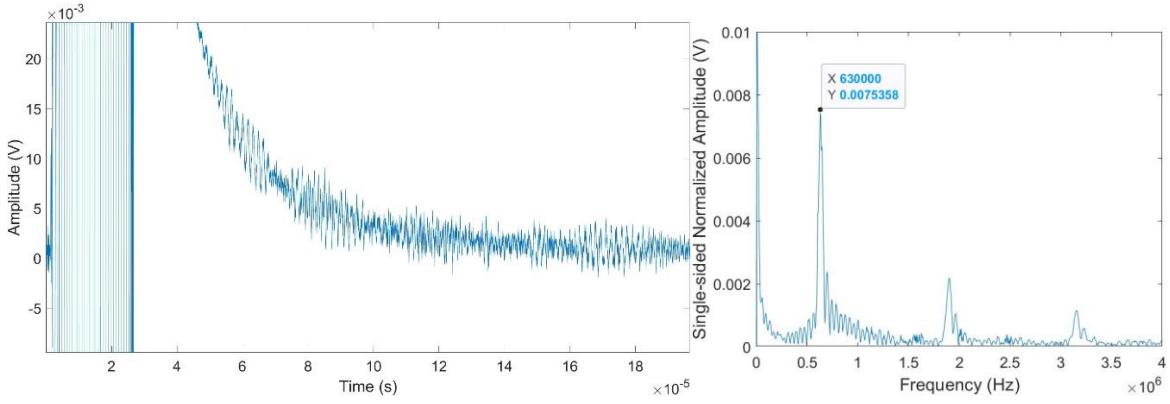

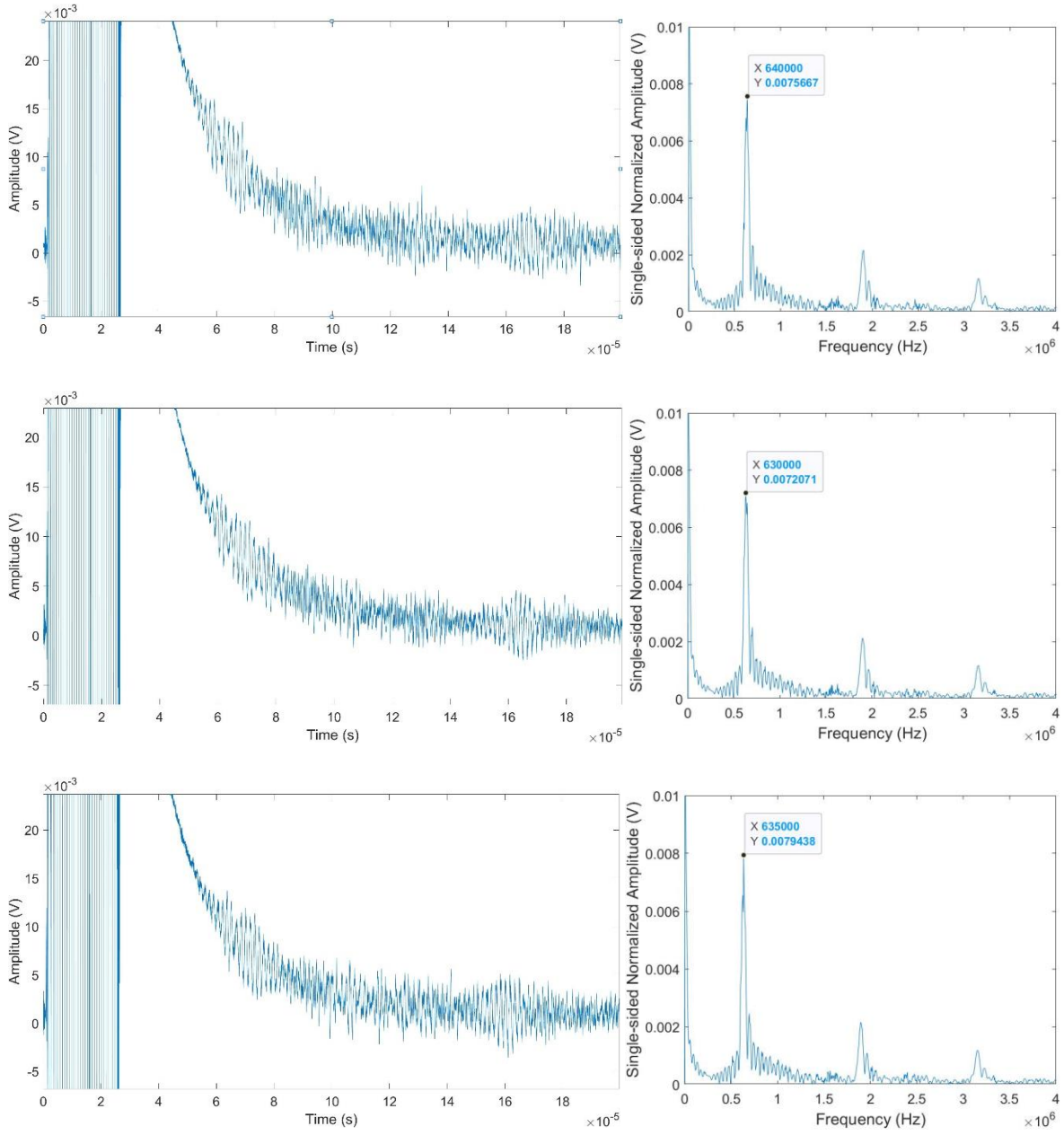

Figure 4.14: A-scans and FFTs of the received signals from 1st, 2nd, 3rd and 4th elements in the receiving transducer

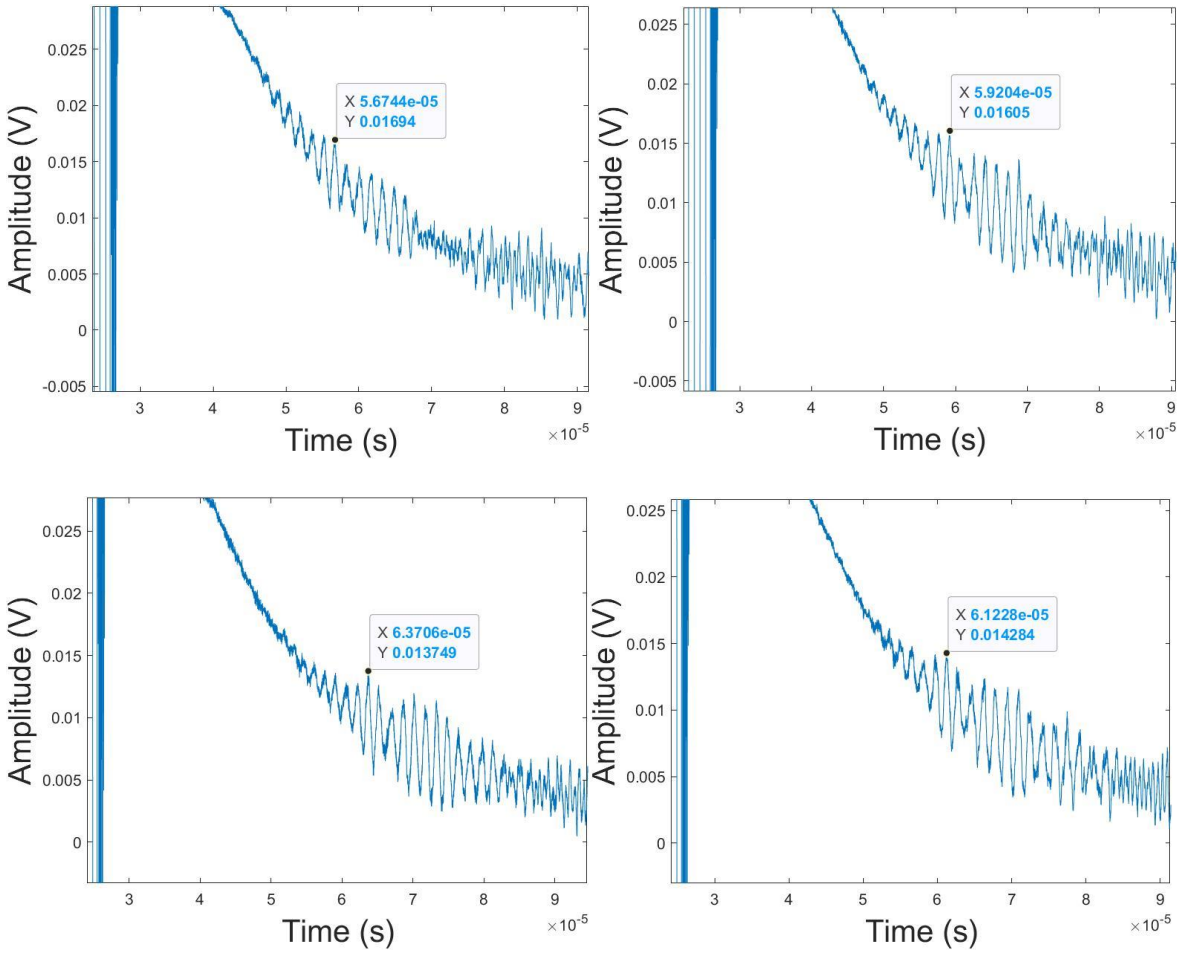

Figure 4.15: The arrival times of mode packets for 1st, 2nd, 3rd and 4th receiving elements (clockwise from top)

Even for a thicker plate, the results are very similar to the ones seen in plates 1 and 2. The waveforms, when received with a farther element, the modes take longer travel time. Here the interference was for a longer time and the first modes arrived around 50 μs as seen in Figure 4.14. The frequency spectra shown in Figure 4.14 confirm that the wave excitation has a frequency of 0.63 MHz for all the elements. Due to the closeness of the actuator to the receiver and a longer wavelength, some initial modes might be lost in the noise as seen in Figure 4.14. A DC offset is introduced in the system due to the amplifier, causing the signal to look such as this (exponentially curving down). It is very hard to accurately identify the start point of any wave packet in this case, so the group velocity was calculated for this plate where the difference between the peaks of the supposed S1 mode packets were selected. With the luxury of 4 receiving elements, the predicted peaks for the S1

mode are shown in Figure 4.15. The difference between the peaks for the first and the fourth elements lead to a time difference of 6.96 µs (63.71-56.75 µs). For an element width of 5 mm, distance between first and fourth element is 30 mm, which gives a C_g for this wave packet as 4.31 mm/µs which is very close to the theoretical S1 mode in Table 4.3. The error % from the theoretical group velocity of the S1 mode is only 3.8 %. As mode differentiation is more difficult than earlier cases analysis for later modes was not carried out.

Plate 3 (configuration 2)

As the actuator and receiver transducers are too close to each other in the first configuration, a second pair was designed which was farther apart and used even more elements. Here 5 elements were used for actuating where 4 elements used for receiving, one after the other.

Table 4.7: Predicted Time-of-Arrival for initial modes for the second configuration of Plate 3 when actuating with five elements and receiving with four elements

TOA prediction (µs)	*1st element*	*2nd element*	*3rd element*	*4th element*
S0	80.84	84.67	88.51	92.34
S1	47.09	49.33	51.56	53.79
A0	70.45	73.79	77.13	80.47
A1	86.29	90.39	94.48	98.57
Distance from actuator (mm)	211	221	231	241

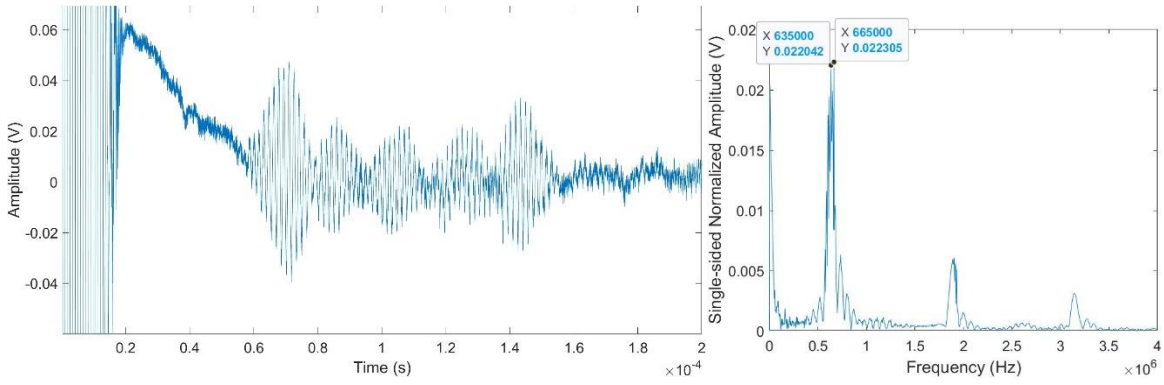

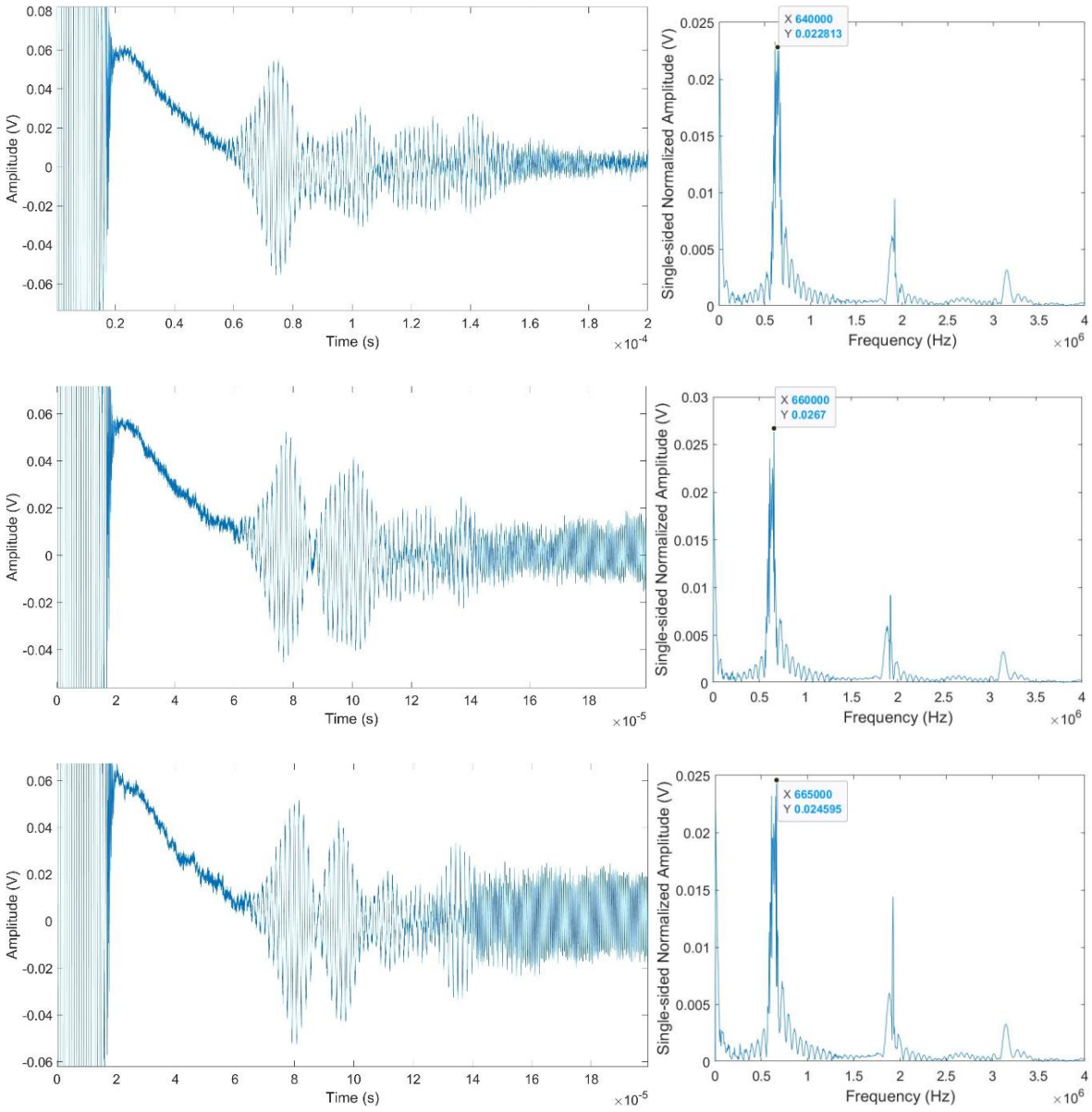

Figure 4.16: A-scans and FFTs of the received signals from 1st, 2nd, 3rd and 4th elements in the receiving transducer

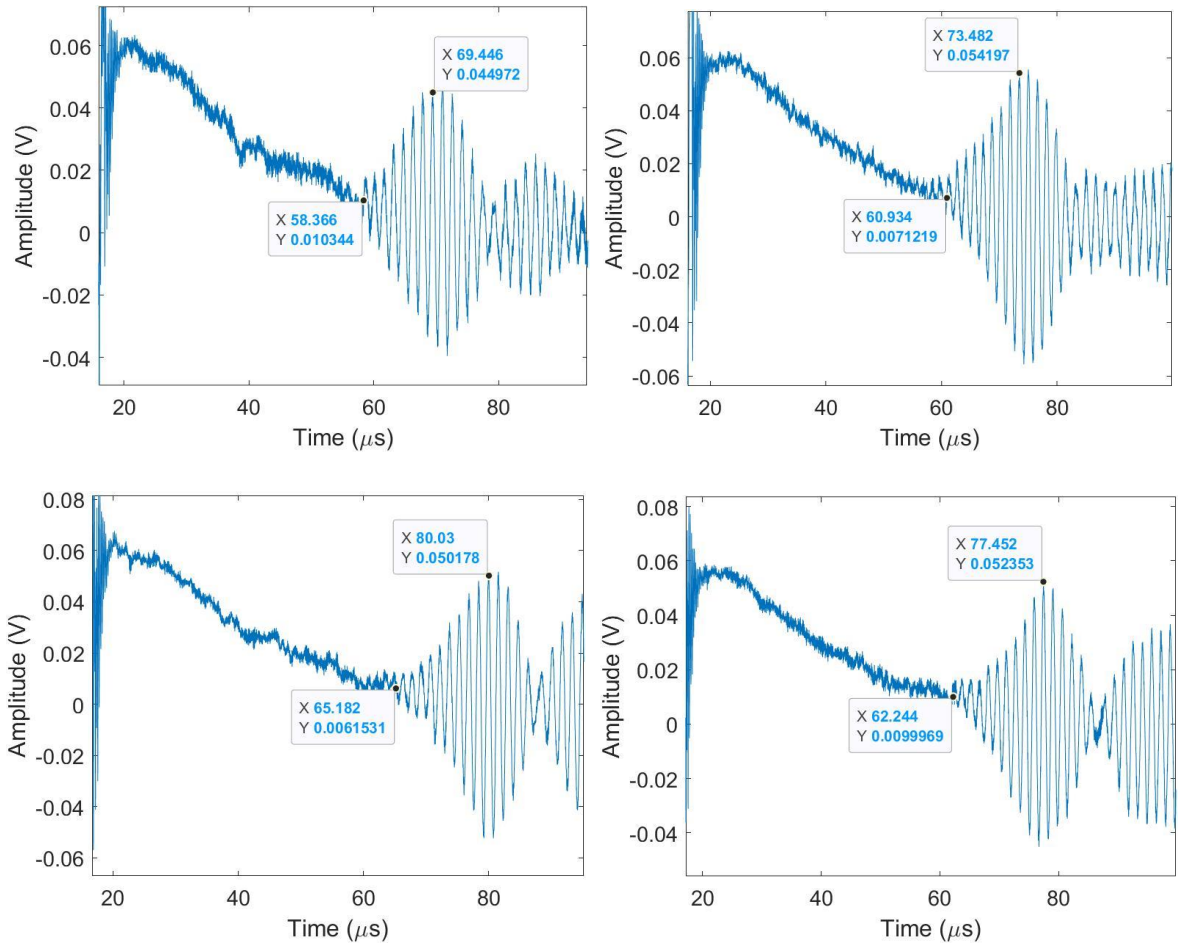

Figure 4.17: The arrival times of mode packets for 1st, 2nd, 3rd and 4th receiving elements (clockwise from top)

Unlike the previous configuration and plate, the FFT plot show that the wave excitation has a frequency of around 0.66 MHz for nearly all the elements which deviated from its excitation frequency of 0.63 MHz Even though this is a bit farther apart from the first configurations, initial modes might still be overlapping. A DC offset is introduced in the system due to the amplifier, causing the signal to look such as Figure 4.16 (exponentially curving down). Here the start times and peaks of a particular travelling wave packet are recorded and shown for each element in Figure 4.17. The difference between the start times for the first and the fourth element is 6.81 μs (65.18-58.37 μs) while the difference between the peaks for the first and the fourth elements is 9.02 μs (80.03-71.01 μs). For an element width of 5 mm, the distance between first and fourth element is 30 mm. From the start time, the C_g is 4.4 mm/μs which has only 1.8 % error from the theoretical C_g for the S1 mode at

4.48 mm/µs. As seen in Table 4.3, the S0, A0 and the A1 mode all have very similar group velocities. The wave packet overlapping the three modes has a C_g of 2.83 mm/µs. There is a noticeable delay in the arrival times as compared to Table 4.7, however from the performed calculations, the received packets are indeed the S1 and other initial modes.

PVDF Dogbone

The dogbone sample had 5 actuating elements and a very thin receiver element.

Table 4.8: Predicted Time-of-Arrival for initial modes for the PVDF sample when actuating with five elements and receiving with only one element

TOA prediction (µs)	*Receiving element*
S0	110.94
S1	64.71
A0	90.09
A1	87.82
Distance from actuator (mm)	271.8

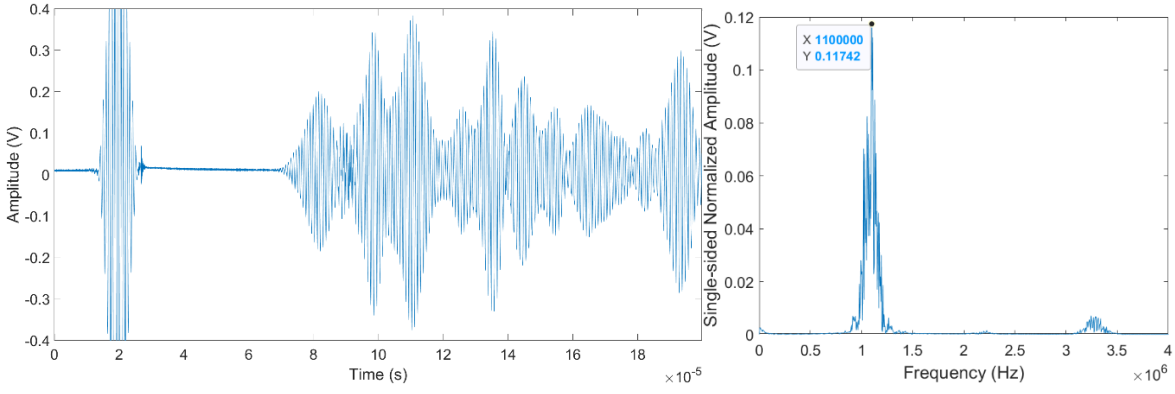

Figure 4.18: A-scans and FFTs of the received signals from 1 element in the receiving transducer

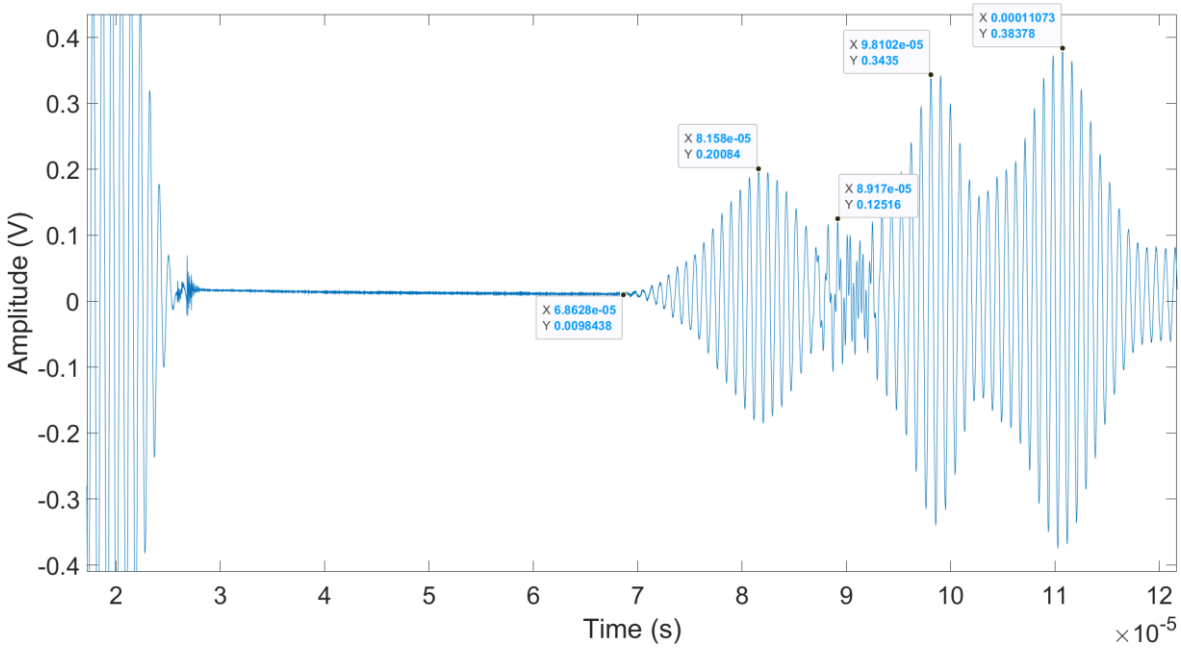

Figure 4.19: The arrival times of the various mode packets for the PVDF sample

Here it is seen that the first arrival mode is 68.78 µs with a delay of 4.07 µs from the predicted S1 mode. Then there is an overlap of the A0 and A1 mode packets but it seems that the A1 mode is arriving at around 91.77 µs with a delay of 3.95 µs. This shows how efficient the PVDF samples are as the delay is nearly constant for the different modes and the noise is minimal in the system.

4.5 Electromagnetic Interference (EMI)

A trigger is a gating signal or pulse which defines a time window so that the signal is only recorded in that time frame and other signals are discarded. An oscilloscope is setup in a way where it starts measuring when a certain condition occurs in the input signal. Triggering is used for capturing and stabilizing repetitive signals instead of measuring at random times. An external trigger from the SNAP system was used to trigger the oscilloscope, however, there were some very anomalous observations. For completeness, shown in Figure 4.21 are the triggers for the 6.4 mm thick plate with BIT film and 3.2 mm thick plate with PVDF

film. It can be seen that there is some unexpected back feed into the trigger causing oscillation. Another noteworthy thing is that the interference shown in the trigger for the BiT films is higher and occurs for a longer time compared to the PVDF film transducer.

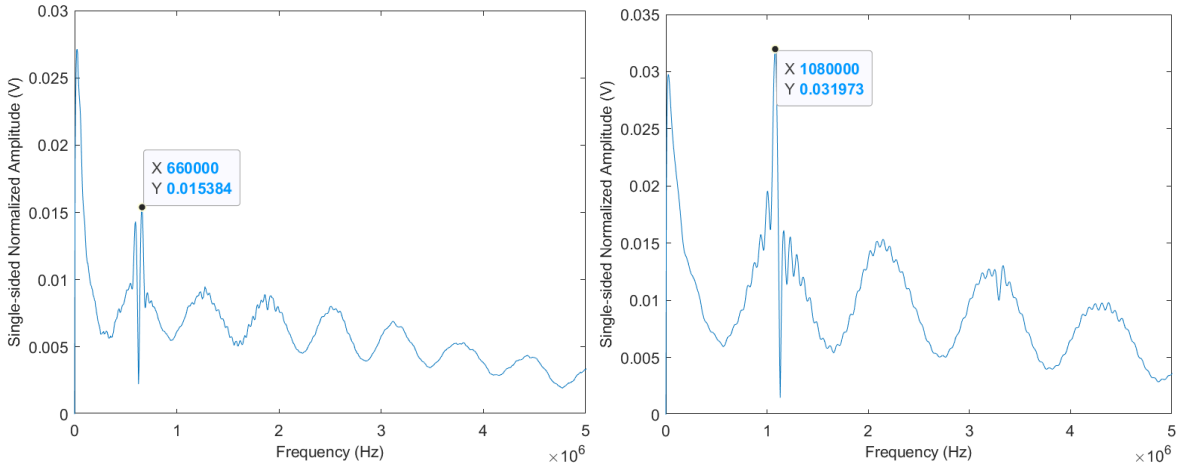

Figure 4.20: FFT of the trigger signal generated from the SNAP system for the 6.4 mm thick plate (left) and 3.2 mm thick plate (right)

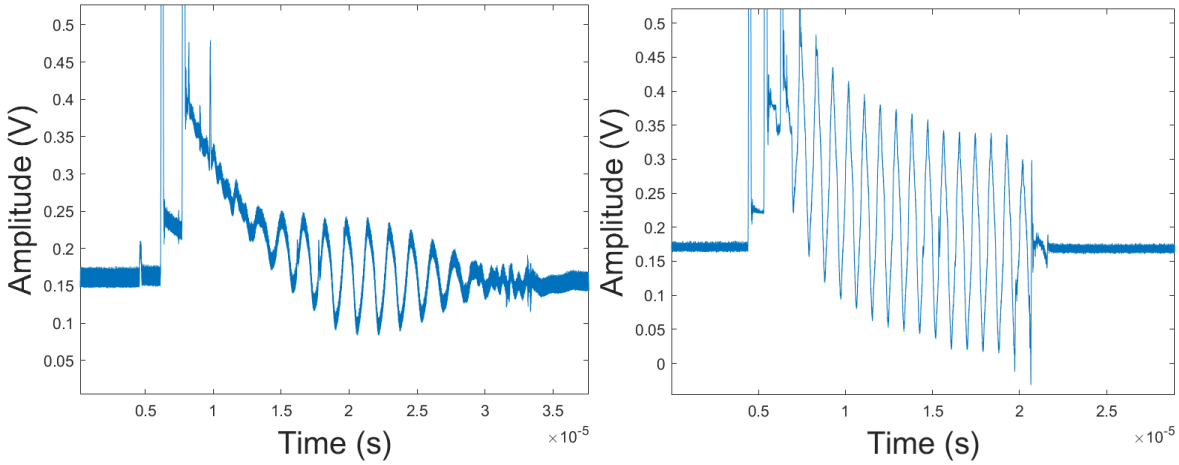

Figure 4.21: Hanning modulated A-scans of the trigger signals from the BIT samples (left) and PVDF samples (right)

Chapter 5 – Conclusion and Future work

This research presented the functionality of piezoceramic film transducers suitable for bulk-wave and guided wave techniques to be used for NDE and SHM. The focus was to create a technology for damage detection in the power and energy industry, where most structures are metallic and operate in a range of temperatures. Compared to previous work by Ledford [8] and Xu [9] where a paint-on (brush-on) technique is used, a spray-on approach was adopted here to better control the film thickness and to ensure its uniformity. The film is prepared by first creating a slurry consisting of the piezo powder, an inorganic binding agent and water in a set concentration and then applied on a surface. Bulk-wave characterization was performed at both room temperature and elevated temperature. Capacitance of the film was measured at room temperature and signal-to-noise ratio was calculated. Three different film types were fabricated: Bismuth Titanate, Lithium Niobate/Barium Titanate and Organic Bismuth Titanate. The final product in all three cases was stable and non-reactive. The fieldable fabrication procedure is straightforward and the materials are non-toxic. Bulk-wave characterization was performed for all three films for comparison. The Bismuth Titanate film is also evaluated for ultrasonic guided wave usage. The novel approaches of using a Lithium Niobate/Barium Titanate transducer and an Organic Bismuth Titanate transducer could have applications of its own. Due to high temperature resistance of the LiN films, detection of hot structures could be easier, however, further work still needs to be performed.

The main goal here was to show guided waves propagation using film transducers on aluminum plates of different thicknesses. A comb transducer arrangement was deposited on the plate surface for pitch-catch measurements. The element width and spacing is dependent on the preferential mode excitation and is equal to half the wavelength of the preferential excited mode. The main conclusions are listed below:

- A Bismuth Titanate film sensor technology is proposed to generate as well as detect guided wave modes through the use of comb transducers
- The fabrication process can be implemented in the field for application on metallic structures

- It is seen that with a greater number of elements used for actuating, the received signal depicts clearer and defined mode [48]
- Results from BIT films compare favorably with a PVDF film in that the BIT films will function at much higher temperatures and do not require as high a voltage to function.

In terms of future work, the aging of the slurry and the film could be an important characterization. High-temperature tests have been performed, but the films have yet to be subjected to sudden temperature changes and the effects of repeated temperature cycling. As majority of the guided wave work has been performed using the BIT, it will be interesting to observe the operation of LiN and the Organic BIT films for guided wave generation and detection. Work on curved surfaces, pipes and other metal structures (Stainless Steel, Iron, Nickel, Titanium) are some bright aspects where these BIT comb transducers can find their applicability. After some considerable efforts, the technology could be introduced for field and high-temperature testing to help perform damage detection in the power industry.

Appendix A: Input Parameters for Bulk-wave

A Panametrics-NDT 5800 pulser/receiver was used for pulse-echo measurements. The settings for all the transducer is shown below.

Table A.1: Pulser/Receiver Settings

Parameter	**Value**
PRF	1.00 kHz
Energy	100 µJ
Damping	25 Ω
HP Filt	1 MHz
LP Filt	10 MHz
Input Attenuation	0.0 dB
Output Attenuation	0.0 dB
Gain	40.0 dB
Sampling Frequency	1 GHz
Time Range	50 µs
Averages	256

Appendix B: Parameters Definition

Here is a definition and function of input parameters and other terms used during data collection from the RITEC system

Trigger: A signal pulsed from the SNAP system to start recording the values from that point onwards

Burst width: The length of the tone-burst generated from the actuator. In this case it was 15 cycles

Excitation frequency: The frequency at which the transducer is excited in order to generate a wave of the similar length as twice the element spacing

Output level: The energy supplied to the actuator when generating the wave, measured in volts

Signal amplifier: Increases the strength of the received signal to clearly see the useful signal or to find the buried signal in noise

Averages: The number of synchronous waveforms averaged before transferring data to a file

Low pass -filter: All the frequencies below the specified number are passed and anything over is filtered

High pass-filter: All the frequencies above the specified number are passed and anything below is filtered

DC offset: An offset in order to display the waveform in the center

Bibliography

1. Rose, Joseph L. *Ultrasonic Guided Waves in Solid Media*. Cambridge University Press, 2014
2. J. David and N. Cheeke. *Fundamentals and Applications of Ultrasonic Waves.* CRC Press, 2002
3. P. J. Schull, B. R. Tittmann. *Non-destructive evaluation: Theory, Techniques, and Applications*. CRC Press, 2002
4. S. O. Reza Moheimani and A. J. Fleming. *Piezoelectric transducers for Vibration Control and Damping.* Springer-Verlag London, 2006
5. A. Arnau. *Piezoelectric Transducers and Applications.* Second Edition, Spring-Verlag Berlin, 2008
6. Z. Nazarchuk. *Acoustic Emissions, Methodology and Applications*. Springer International Publishing AG, 2017, Chapter 2
7. H. Cho, "Toward Robust SHM and NDE of Plate-like Structures using Nonlinear Guided Wave Features", Ph. D Thesis, 2017. The Pennsylvania State University, University Park, PA
8. K. R. Ledford, "Practical sprayed-on transducer composites for high temperature applications", Master's Thesis, 2015. The Pennsylvania State University, University Park, PA
9. J. L. Xu, "Practical Ultrasonic Transducers for High Temperature Applications using Bismuth Titanate and Ceramabind 830", Master's Thesis, 2017. The Pennsylvania State University, University Park, PA
10. A.R. Lesky, "Structural Health Monitoring of Shell Structure using Piezoelectric Fiber Composite Strip Transducers", Master's Thesis, 2014. The Pennsylvania State University, University Park, PA
11. N. Malarich, "Spray-on comb transducers for health monitoring of high temperature structures," Bachelor's Thesis (2015), The Pennsylvania State University, University Park, PA

12. C.T. Searfass, "Fabrication and Testing of Piezoelectric Bismuth Titanate for use as a high Temperature Ultrasonic Transducer" Master's Thesis, 2008. The Pennsylvania State University, University Park, PA
13. I. A. Viktrov. *Rayleigh and Lamb Waves, Physical Theory and Applications*. Springer Publishing US, 1967
14. D. Barrow, T. Petroff, and M. Sayer, “Thick ceramic coatings using a sol-gel based ceramic-ceramic 0-3 composite,” Surface and Coatings Technology, 76 (1995), pp. 113 – 118
15. Kobayashi, M. and C.-K. Jen “Piezoelectric thick bismuth titanate/lead zirconate titanate composite film transducers for smart NDE of metals,” Smart Materials and Structures, 13(4) (2004), p. 951.
16. C.J. Borigo, “Excitation Spectrum & Mode Excitability Analysis of Comb and Annular Phases Array Transducers for Guided Wave Mode Control Applications”, Master’s Thesis, 2011. The Pennsylvania State University, University Park, PA
17. N. Das, H. S. Maiti, “Ceramic membrane by tape casting and sol-gel coating for microfiltration and ultrafiltration application”, Journal of Physics and Chemistry of Solids, 70 (2009), pp. 1395-1400
18. K. Lindqvist, E. Liden, “Preparation of Alumina Membranes by Tape Casting and Dip Coating”, Journal of the European Ceramic Society, 17 (1997), pp. 359-366
19. K. L. Gentry, J. M. Zara, S. D. Bu, C. B. Eom, S. W. Smith, “Thick-Film Sol-gel PZT Transducer using Dip-coating”, IEEE Ultrasonics Symposium, 2000, pp 977-980
20. J. Sumerel, J. Lexis, A. Doraiswamy, L. F. DEravi, S. L. Sewell, A. E. Gerdon, D. W. Wright, R. J. Narayan, “Piezoelectric ink-jet Processing of Materials for Medical and Biological Applications”, Biotechnology Journal, 1(2006), pp. 976-987
21. Herbert, J.M. *Ferroelectric Transducers and Actuators*. New York: Gordon and Breach Science Publishers, 1982. Page 6, 42, 43
22. Silk, M.G. Ultrasonic Transducers for Nondestructive Testing. Adam Hilger Ltd. 1984. Page 21.

23. A. Jain, S. J. Kumar, M. R. Kumar, A. S. Ganesh, S. Sriaknth, “PVDF-PZT Composite Films for Transducer Applications”, Mehancis of Advanced Materials and Structures, 21 (2014), pp. 181-186
24. P. Giannelli, A. Bulletti, L. Capineri, “Multifunctional Piezopolymer Film Transducer for SHM Applications”, IEEE Sensors Journal, Vol 17, 14 (2017), pp. 4583-4586
25. Yi, G. and M. Sayer *Sol-Gel Processing of Complex Oxide Films*, Ceramic Bulleting, Vol 70, 7 (1991), pp. 1173-1179
26. K. M. Sinding, “The effect of weight percent on the properties of ultrasonic transducers fabricated though a sol-gel deposition process,” Bachelor’s Thesis (2014), The Pennsylvania State University, University Park, PA
27. A. Orr, “A bond stiffness study of sol-gel spray-on transducers”, Master’s Thesis (2015), The Pennsylvania State University, University Park, PA 16802.
28. J. L. Rose, *Ultrasonic Guided Waves in Structural Health Monitoring*, Key Engineering Materials Vols. 270-273 (2004) pp.14-21
29. R. S. Weis, T. K. Gaylord, “Lithium Niobate: Summary of Physical Properties and Crystal Structure”, Applied Physics, A 37 (1985), pp. 191-203
30. P. Gupta, Balram, D. P. Singh, “Synthesis and Characterization of Ferroelectric Bismuth Titanate”, Solid state Physics, AIP Conference Proceedings 1591 (2014), pp. 565-567
31. B. J Kim, C. S. Kim, D. J. Kim, H. H. Lim, S. K. Park, M. Cha, K. J. Kim, “Fabrication of Thick Periodically-poled Lithium Niobate Crystals by Standard Electric Field Poling and Direct Bonding”, Journal of the Optical Society of Korea, Vol 14, 4 (2010), pp. 420-423
32. Uitert, L. G. V. and L. Egerton “Bismuth Titanate. A Ferroelectric,” Journal of Applied Physics, Vol 32, 5 (1961), pp. 959–959
33. K. V. Arunkumar, “Dispersion and Rheological Characterization of TiO_2 Tape Casting Slurry”, International Journal of Applied Ceramic Technology, Vol 7, 6 (2010), pp. 902-908
34. F. A. Vargas, R. Z. Ulloa, Point-Defect Chmistry on the polarization behavious of Niobium Doped Bismuth Titanate

35. Safari, A: Akdogan, E.K. “Piezoelectric and Acoustic Materials for Transducer Applications”. Springer. 2008. Page 22.
36. Simoes, A.Z. “Ferroelectric and Piezoelectric properties of Bismuth Titanate thin films grown on dierent bottom electrodes by soft Chemical Solution and Microwave Annealing. Materials Research Bulletin, 2007.
37. R.C. Eckardt, H. Masuda, Y.X. Fan, and R.L. Byer IEEE Journal of Quantum Electronics 26(5), 922 (1990)
38. T. R. Hay, J. L. Rose, “Flexible PVDF comb transducers for excitation of axisymmetric guide waves in pipe”, Sensors and Actuators A 100 (2002) pp. 18-23
39. D. Damjanovic, Materials for high temperature piezoelectric transducers. Current Opinion in Solid State and Materials Science, Vol 3, Issue 5 (1998), pp 469-473
40. T Dargaville, M Celina, J. Elliott, P Chaplya, “Characterization, performance and Optimzation of PVDF as a Piezoelectric Film for Advanced Space Mirror Concept”, Sandia National Laboratories (2005), Report SAND2005-6846
41. J. C. Brice, “The Properties of Lithium Niobate”, EMIS Data reviews Series No.5, The Institute of Electrical Engineers (1989)
42. URL: https://www.comsol.com/blogs/piezoelectric-materials-crystal-orientation-poling-direction/
43. URL: https://docplayer.net/11201172-Solutions-for-nuclear-technology.html
44. URL: https://docplayer.net/4658999-Advanced-ndt-solutions-oil-gas-products-systems-services.html
45. URL: http://docplayer.net/78491857-Ultrasonic-techniques-for-testing-transportation-containers-and-pipelines.html
46. URL: https://www.infrastructurepc.com/ndtoftanks/
47. URL: https://en.wikipedia.org/wiki/Guided_wave_testing
48. J. L. Rose, S. P. Pelts, M. J. Quarry, “A Comb Transducer Model for Guided Wave NDE” Ultrasonics 36 (1998) pp. 163-169
49. J. J. Ditri, J.L. Rose, A. Pilarski, “Generation of Guided Waves in Hollow Cylinders by Wedge and Comb Type Transducers”, Review of Progress in Quantitative Nondestrictive Evaluation, pp. 211-218

50. T. Hay, “Design Considerations and Applications for Comb Transducers used in Nondestructive Evaluation”, Master’s Thesis, 2001. The Pennsylvania State University, University Park, PA.
51. C. S Morandi, “The Effect of Secondary Phases and Birefringence on Visible Light Transmission in Translucent α’-Sailon Ceramics”, Master’s Thesis, 2014, The Pennsylvania State University, University Park, PA
52. K. J. Kirk, J. Elgoyhen, J. P. Hood, D. Hutson, “Use of Mas Loading to operate a Thin Films Ultrasonic Transducer in the 300 kHz-10 MHz frequency range” Journal of Electroceramics, Vol 21, Issue 1 (2011), pp29-32
53. C. Brinker, G. Scherer, *Sol-Gel Science, The Physics and Chemistry of Sol-Gel Processing*, Academic Press, 2013
54. C. Galassi, E. Roncari, C. Capiani, P. Pinasco, “PZT-based Suspensions for Tape Casting” , Journal of European Ceramic Society, 17 (1997), pp. 367-371